

## Theory of gas lasers operating on two coupled transitions

A. H. Paxton\*

*Air Force Weapons Laboratory, Kirtland Air Force Base, New Mexico 87117*

P. W. Milonni

*Department of Physics, University of Arkansas, Fayetteville, Arkansas 72701*

(Received 27 August 1981)

The semiclassical Lamb theory of gas lasers is extended to the case of lasers operating simultaneously on two coupled transitions. The theory is formulated in terms of the density-matrix equations for a three-level gaseous laser medium interacting with the field through electric-dipole transitions, so that there are two allowed transitions and one two-photon transition. It is assumed that there is a single resonator mode near each of the transition frequencies. Previous treatments of such three-level gas lasers either have used simple rate equations or have solved the density-matrix equations in an approximate fashion valid only for low intensities. Thus the numerical approach developed herein represents, to our knowledge, the first semiclassical theory of three-level gas lasers which is accurate for arbitrary detuning and intensity. Significant deviations from earlier, approximate treatments are found.

### I. INTRODUCTION

In describing the resonant interaction of light with an atom or molecule, it is often a very accurate approximation to include in the analysis only those discrete energy levels that define the resonant transitions. If the resonant radiation is nearly monochromatic, for instance, the model of the "two-level" atom is extremely useful.<sup>1,2</sup> The well known and highly successful Lamb theory of the gas laser is based on the treatment of the laser medium as a collection of two-level atoms.<sup>1,3</sup>

There has recently been considerable interest in the resonant interaction of light with three-level atoms or molecules. (See Refs. 4–8 and the references cited therein.) The analysis of the three-level system is more complicated than the two-level case, and certain aspects of the problem have consequently not been carefully analyzed. This is especially true for the case of the three-level laser operating simultaneously on two coupled transitions of a Doppler-broadened gaseous gain medium. Beterov and Chebotaev noted in 1975 that "In a three-level gas oscillator, the picture of saturation effects becomes considerably more complicated (than in a two-level system) and at present there is no theory of a three-level gas laser."<sup>4</sup> A low-intensity theory of the three-level gas laser was published in 1975.<sup>9</sup> It is our purpose to present a more general theory.

The motivation for this work has been to develop a more complete understanding of lasers which operate on multiple transitions. A number of gas-laser gain media consist of atoms or molecules with three or more states which are all coupled by allowed transitions in a cascading configuration. Some examples are CO, He-Ne, DF, and HF. The existence of several coupled transitions will influence the laser gain and index of refraction by causing the level population and the induced polarization oscillations to have complicated spatial variations along the direction of propagation of the light (the  $z$  axis). The spatial variation of any of the level populations will contain harmonics of the wave numbers of all the laser modes.

In the two-transition laser there are effects associated with the direct coupling of the laser modes by the density-matrix element connecting the two levels between which there is no allowed transition. The third-order semiclassical theory of the response of a three-level gain medium indicated that these coupling effects are significant.<sup>10</sup> The analysis of a three-level gas with a high-intensity laser beam saturating one transition has also shown that these coherence effects qualitatively change the line shape.<sup>11–14</sup> The third-order laser theory of Najmabadi *et al.*<sup>9</sup> showed that peaks in plots of mode intensity as a function of laser tuning near line center were caused by these coupling effects. This treat-

ment did not, however, explore a wide range of values of the relative tuning of the modes, and moreover the third-order theory is only valid at low intensity.

As the simplest example of the multitransition cascading laser, the three-level laser will provide insight into this class of laser. It is also possible to construct two-transition lasers for which our idealized model is a good approximation.

Recently, such lasers have been used to investigate the possibility of using cascading Ne transitions to obtain a tunable laser.<sup>15,16</sup> Standing-wave and traveling-wave lasers were operated with a single longitudinal mode resonant with each of two coupled transitions over a range of detunings, and numerical results ignoring population pulsations were presented.

There are various levels of analysis at which one can approach the theory of gas lasers. For instance, the theory of laser oscillation can be formulated simply in terms of rate equations for the relevant atomic or molecular energy levels. The overall power output of gas lasers can often be modeled fairly well, although certain effects, such as mode locking, find no explanation in this approach.

The rate-equation approximation is normally used when the importance of hydrodynamic effects and intensity nonuniformity in the laser make a more detailed treatment of the density-matrix equations impractical. Engineering codes used for the design of high-power gas lasers always use this approximation. In the engineering codes, detailed rates for all excitation and deexcitation processes are coupled with a hydrodynamics model sufficiently detailed to treat the gas flow and obtain values of pressure and temperature on which the rates depend. The cavity fields are obtained by coupling a physical-optics (Fresnel propagation) or geometric-optics model to the rate equations. At one or more planes normal to the resonator axis (gain sheets), the electromagnetic field intensity distribution is input to the gain medium model to obtain a new intensity distribution. The field is then propagated to the next gain sheet after reflecting from any intermediate mirrors. This calculation is iterated until several successive round-trip propagations yield identical results. Such codes have become important in the design of high-power lasers, and several models have been described in the literature.<sup>17-19</sup>

On the other hand, semiclassical analyses of laser oscillation, including the detailed treatment of the density-matrix equations, have generally ignored the spatial variation of the laser intensity transverse to the resonator optic axis, as well as any complicated

hydrodynamic effects. The density-matrix equations are sufficiently complex that the incorporation of these additional effects makes the problem exceedingly difficult from a computational, if not conceptual, point of view.

In the Lamb theory of the single-transition laser, the gain medium is represented by the decay rates of the two atomic levels, together with the width of the Doppler broadening due to the velocity distribution of the gas. Intensities are specified as dimensionless ratios involving the dipole moment of the transition, and the gain is specified as a dimensionless ratio involving the pumping rates and decay rates. The decay rates and the pumping rates are usually considered to be constant both in time and in space. Phase effects such as mode locking and frequency pulling (the contribution to the index of refraction due to the resonant interaction) are modeled. Polarization components corresponding to harmonics of the cavity modes are generated due to the coupling of the off-diagonal terms of the density matrix with the diagonal terms.

The semiclassical density-matrix formalism used here is similar to the two-level theory of Lamb *et al.*,<sup>1,3,20</sup> and the three-level theory of Najmabadi, Sargent, and Hopf.<sup>9</sup> Phenomenological decay rates and level-pumping rates are included. Population pulsations<sup>1</sup> and coherence between the two transition amplitudes are also treated. This is an extension of previous work in that we have derived a partial-difference equation for the density-matrix elements which is valid for arbitrary intensity and detuning of either mode. This difference equation was solved numerically using a matrix method, and the results were averaged over the velocity distribution. Our calculated results consist of an average gain and index of refraction corresponding to each mode. By using a method of successive approximation, we have also calculated the self-consistent amplitudes of the two laser modes.

Some of the structure of the three-level gas laser can be qualitatively understood by applying the hole-burning arguments of Bennett.<sup>21</sup> Figure 1 shows the assumed level scheme. Suppose that lasing is occurring into a mode resonant with transition  $b$ , which is detuned from line center by  $-\Delta_b$ . Then the velocity distribution of the population of level three is depleted in the vicinity of  $v_h = \Delta_b/k_b$  and  $-v_h$ , because these velocity groups are Doppler shifted into resonance with the mode.  $k_b$  is the wave number of the mode. Similarly, the velocity distribution of the population of level two is increased in the vicinity of  $\pm v_h$ . The velocity distribution of the population inversion of transition  $b$

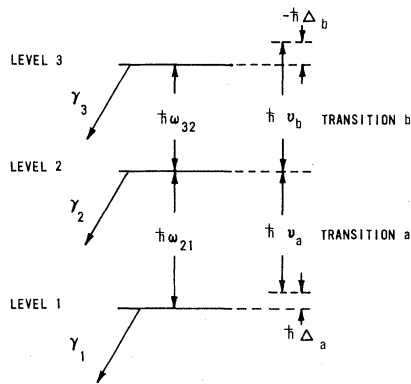


FIG. 1. Cascading level scheme. The dashed lines at the right of the figure show the amounts by which the laser modes are detuned from the center frequency of the atomic resonance.

therefore has two Lorentzian holes, called Bennett holes, burned into it at velocities  $\pm v_h$ .

Level two is the upper level for transition *a*, so the velocity distribution of the population inversion of transition *a* is a Maxwell distribution with two Lorentzian bumps superimposed at velocities  $\pm v_h$ . Figures 2(a) and 2(b) show the nonequilibrium velocity distributions of the population inversions of transitions *a* and *b*, respectively. When the mode resonant with transition *a* is tuned through  $\Delta_a = \pm k_a \Delta_b / k_b$  (while  $\Delta_b$  is kept constant), an intensity bump will result from a bump on the

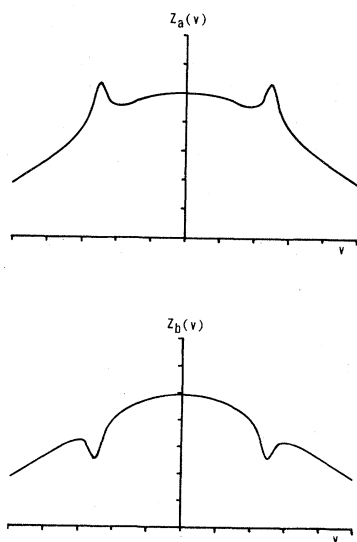


FIG. 2. Velocity distributions of population inversions of transition *a* and transition *b*, influenced by an intense standing-wave field resonant with transition *b*.

population-inversion distribution. This structure has been used to determine the frequency of a transition within an error which is much less than the Doppler width. (See, for example, Ref. 22).

These intensity bumps occur in the detailed theory, but there are also features which cannot be explained using only population-inversion arguments. Raman-type terms arising from the density-matrix element connecting level one with level three can cause a splitting of one of the resonances under certain circumstances. They also cause the intensity bump at  $\Delta_a$  to have a different width than the bump at  $-\Delta_a$ .

In this paper we consider a Fabry-Perot resonator with nearly perfectly reflecting mirrors. Because the transverse electric field vanishes at the mirrors, the resonator modes are standing waves with wavelengths  $\lambda_i = 2L/N_i$ , where the  $N_i$  are large integers and  $L$  is the separation of the mirrors. The vacuum (circular) frequency separation of the modes,  $\Delta\Omega = \pi c/L$ , is always much greater than the frequency width of a cavity mode. The cavity mode widths are also much smaller than the atomic homogeneous line widths, so they are small compared to the size of any structure in the lasing transition line shape. Therefore the cavity modes are assumed to have zero width for the purpose of the calculation.

The calculation of the intensities and frequencies of laser modes is performed as follows. The polarization induced by a combination of cavity modes is calculated using quantum mechanics. Then Maxwell's equations are used to derive the cavity modes resulting from the polarization. Requiring the cavity modes to be consistent with the induced polarization (self-consistency) fixes the intensities and frequencies of the various modes. This is the condition of self-consistency in the semiclassical Lamb theory.

Some of the most salient assumptions and approximations used in the present work are the following. (i) A single linear polarization is assumed for the field. (ii) The two transitions are predominantly Doppler broadened. (iii) The atomic velocity distribution is Maxwellian. (iv) The pumping mechanisms for establishing the population inversions are specified only by constant rate coefficients. (v) Population deexcitation mechanisms are modeled by phenomenological rates, as are the off-diagonal "dipole-dephasing" terms that give rise to homogeneous line broadening. (vi) Collisions are ignored, except insofar as they contribute to the homogeneous linewidths of the transitions.

Assumption (i) is valid whenever Brewster win-

dows are used at the ends of the gain cell. Assumption (ii) is valid in low-pressure gaseous lasers such as He-Ne, which typically has a gas pressure on the order of one Torr. The 6328-Å Ne transition, for example, has a Doppler width (FWHM) of about 1.7 GHz, whereas spontaneous emission and collisions contribute widths of about 20 MHz and 1 MHz, respectively, to its homogeneous linewidth. Assumption (iii) is expected to be valid to a very high degree of accuracy, since the thermalizing elastic atom-atom collisions are more frequent than inelastic collisions. The electron velocity distribution will generally be non-Maxwellian, but this is of no consequence to assumption (iii), as the electron number densities are very low compared with the neutral heavy particles.

Approximations (iv) and (v) are excellent when a flash lamp provides the pumping and only spontaneous emission is involved in the decay of the resonant levels, for then we have simple linear rate processes. Energy-transfer processes, however, such as those between He and Ne in the He-Ne laser, are not as easy to treat. The chemical-kinetics equations for these processes are nonlinear. There is typically about ten times as much He as the lasing Ne, so there is some justification for regarding the He as a background, unperturbed bath in its interaction with the Ne. But in general, the modeling of pumping and deexcitation processes by simple linear rate constants is only a crude approximation made for the sake of analytical simplicity. The success of semiclassical laser theory does indicate, however, that (iv) and (v) are not terribly restrictive approximations.

Approximation (vi) may be invalid even when assumption (ii) is satisfied. This is because elastic collisions change the projections of the velocities of the colliding atoms on the laser optic axis. If the elastic-collision rate is comparable to the stimulated emission rate, the selective saturation of the population inversion of atoms in specific velocity intervals will be partially washed out. In low-pressure lasers, however, the lasing rate is typically much larger than the collision rate, and (vi) is a good approximation for such systems.

The next section summarizes our formalism for the three-level, two-transition gas laser. In Sec. III, some approximations used in previous work are discussed for later comparison with our exact results. Section IV describes briefly the numerical techniques used to solve the basic difference equations

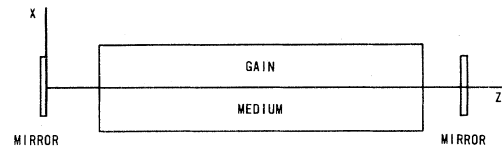


FIG. 3. Laser cavity geometry.

of the theory developed in this work. Solutions for the laser intensities in terms of the gain and detuning are presented and compared with results of the standard approximations for various cases of interest. Preliminary results have been published elsewhere.<sup>23</sup> Section V is a brief summary of the major conclusions drawn from this work.

## II. SEMICLASSICAL FORMALISM FOR THE INTERACTION OF RADIATION WITH A THREE-LEVEL LASER MEDIUM

Our treatment of the three-level laser is analogous to the two-level analyses of Stenholm and Lamb<sup>20</sup> and Feldman and Feld.<sup>24</sup> The three-level atoms are assumed to interact with two standing-wave modes. Each mode is resonant with one of the two allowed transitions. We use a density-matrix formalism, and the steady-state density-matrix elements are expanded in the  $z$  coordinate (see Fig. 3) in harmonics of the wave numbers of the two modes. The density-matrix elements are obtained numerically for assumed amplitudes of the laser modes, and are averaged over the atomic velocity distribution.

The gain of each mode is obtained from the averages. In a laser cavity, the physical situation is for the intensity of each mode to reach a steady state only when its gain is equal to the cavity losses. These losses are specified by the cavity  $Q$ 's (quality factors). Satisfying this self-consistency condition numerically is complicated in the three-level case by the dependence of the gain of one mode on the amplitude of the other mode. In our work an iterative method is used to adjust the intensities until the desired gain was obtained for each mode. Continuous-wave (i.e., steady-state) operation of the laser is assumed.

The electromagnetic field is written in the form

$$E = \hat{x} \left[ (4 |A_a| \hbar / \mu_a) \cos(\nu_a t + \theta_a) \sin(k_a z) + (4 |A_b| \hbar / \mu_b) \cos(\nu_b t + \theta_b) \sin(k_b z) \right], \quad (2.1)$$

where  $A_a = |A_a| e^{i\theta_a}$  and  $A_b = |A_b| e^{i\theta_b}$ .  $A_a$  and  $A_b$  will have no time dependence in this treatment, although the density-matrix equations below are valid even if  $A_a$  and  $A_b$  are slowly varying in time compared with the sinusoidal oscillations at frequencies  $\nu_a$  and  $\nu_b$ .  $\mu_a$  and  $\mu_b$  are the transition dipole moments and may be assumed to be real numbers.  $\hat{x}$  is a unit vector transverse to the optic axis ( $z$  axis) of the resonator. Both laser modes are assumed to have the same linear polarization due to polarizing elements within the cavity such as windows which are at an angle with the propagation direction. Equation (2.1) assumes that one of the cavity end mirrors is located at  $z=0$ . Both of the (standing-wave) modes have nodes at  $z=0$ .

Phenomenological pumping and decay rates are used in the density-matrix equations. Thus the diagonal density-matrix elements with the interaction Hamiltonian  $V = \vec{\mu} \cdot \vec{E}$  satisfy the equations

$$i\hbar\dot{\rho}_{jj} = -i\hbar\gamma_j(\rho_{jj} - n_j) + \sum_m (V_{jm}\rho_{mj} - V_{mj}\rho_{jm}), \quad (2.2)$$

where  $\gamma_j$  is the rate at which the population of level  $j$  relaxes to the steady-state value  $n_j$  in the absence of an electromagnetic field. In general,  $\gamma_j$  will be the sum of a spontaneous decay rate and a decay rate due to inelastic collisions. Similarly, the off-diagonal density-matrix equations are

$$i\hbar\dot{\rho}_{jn} = \hbar\omega_{jn}\rho_{jn} - i\hbar\beta_{jn}\rho_{jn} + \sum_m (V_{jm}\rho_{mn} - V_{mn}\rho_{jm}). \quad (2.3)$$

The decay rates for  $\rho_{ij}$ ,  $i \neq j$ , are  $\beta_{ij} = \frac{1}{2}(\gamma_i + \gamma_j)$  if the gas pressure is low enough that the spontaneous emission rate is much larger than the collision rate of the excited atoms.<sup>2</sup> The  $\beta$ 's are the rates at which the oscillations of the atomic dipoles are interrupted due to the decay of the stationary states. Elastic collisions also contribute to the dephasing of the oscillations so, in general,  $\beta_{ij} \geq \frac{1}{2}(\gamma_i + \gamma_j)$ .<sup>2</sup>

An elastic collision can also change the projections of the velocities of the atoms on the  $z$  axis, and therefore cannot simply be represented as an increase in the  $\beta_{ij}$ .<sup>25,26</sup> Our treatment will include the effects of elastic collisions only insofar as they can be treated by increasing the  $\beta_{ij}$ .

A number of terms which occur in the products  $V_{jm}\rho_{jm}$  in Eqs. (2.2) and (2.3) may be neglected. For instance, if we consider  $\rho_{21}$  to consist of a number of frequency components such as  $\rho_{21}^{\pm a} \exp(\pm i\nu_a t)$  and  $\rho_{21}^{\pm b} \exp(\pm i\nu_b t)$ , then  $\rho_{21}^a$  is the only coefficient which has a nonnegligible magnitude. Similarly,  $\rho_{32}$

may be assumed to have time dependence  $\exp(-i\nu_b t)$  and  $\rho_{31}$  to have time dependence  $\exp[-i(\nu_b + \nu_a)t]$ . The only components of  $\rho_{11}$ ,  $\rho_{22}$ , and  $\rho_{33}$  with significant magnitudes have no time dependence. We therefore omit some of the nonresonant terms of the potentials  $V_{jm}$  that would lead to other frequencies.

We consider a group of atoms moving with the component of velocity  $v$  along the  $z$  axis. The total time derivative is then given by the convective derivative,  $d/dt = \partial/\partial t + v\partial/\partial z$ . The density-matrix equations obtained by replacing the time derivative in Eqs. (2.2) and (2.3) by the convective derivative, and omitting terms with nonresonant time dependence, are well known and will not be reproduced here. The equations for the density-matrix elements have solutions of the form

$$\rho_{21} = e^{-i\nu_a t} \sum_{j,n} F_{jn}(v) e^{i(jk_a + nk_b)z}, \quad (2.4)$$

$$\rho_{32} = e^{-i\nu_b t} \sum_{j,n} G_{jn}(v) e^{i(jk_a + nk_b)z}, \quad (2.5)$$

$$\rho_{31} = e^{-i(\nu_a + \nu_b)t} \sum_{j,n} S_{jn}(v) e^{i(jk_a + nk_b)z}, \quad (2.6)$$

$$\rho_{11} = \sum_{j,n} B_{jn}(v) e^{i(jk_a + nk_b)z}, \quad (2.7)$$

$$\rho_{22} = \sum_{j,n} C_{jn}(v) e^{i(jk_a + nk_b)z}, \quad (2.8)$$

$$\rho_{33} = \sum_{j,n} D_{jn}(v) e^{i(jk_a + nk_b)z}. \quad (2.9)$$

All the sums in Eqs. (2.4) through (2.9) run from  $j, n = -\infty$  to  $\infty$ . The coefficients  $F_{jn}$  and  $G_{jn}$  are traveling-wave polarization components resonant with transitions  $a$  and  $b$ , respectively. In particular,  $F_{1,0}$  and  $F_{-1,0}$  are the coefficients of right-traveling and left-traveling polarization waves with the same spatial frequency as the traveling waves into which the standing-wave electromagnetic field can be decomposed. The  $G_{0,\pm 1}$  have similar relationships with the electromagnetic field resonant with transition  $b$ .

To make our notation more compact, we let

$$\Delta_a = \omega_{21} - \nu_a,$$

$$\Delta_b = \omega_{32} - \nu_b,$$

$$\Delta_c = \Delta_a + \Delta_b,$$

$$\beta_a = \beta_{21},$$

$$\beta_b = \beta_{32},$$

$$\beta_c = \beta_{31}.$$

We also find it convenient to define generalizations of complex Lorentzian denominators,

$$L_{jm}^a = i[\Delta_a + v(jk_a + mk_b)] + \beta_a,$$

$$L_{jm}^b = i[\Delta_b + v(jk_a + mk_b)] + \beta_b,$$

$$L_{jm}^c = i[\Delta_c + v(jk_a + mk_b)] + \beta_c,$$

$$M_{jm}^m = i(jk_a v + nk_b v) + \gamma_m.$$

Difference equations for the coefficients of the steady-state solutions are obtained by using (2.4) through (2.9) in the density-matrix equations (2.2) and (2.3). After making the rotating-wave approximation and ignoring other terms which are far off resonance, these difference equations are found to be

$$M_{jn}^1 B_{jn} = A_a(F_{j-1,n} - F_{j+1,n}) + A_a^*(F_{-j-1,-n}^* - F_{-j+1,-n}^*) + \gamma_1 n_1 \delta_{j,0} \delta_{n,0}, \quad (2.10)$$

$$M_{jn}^2 C_{jn} = -A_a(F_{j-1,n} - F_{j+1,n}) - A_a^*(F_{-j-1,-n}^* - F_{-j+1,-n}^*) + A_b(G_{j,n-1} - G_{j,n+1}) + A_b^*(G_{-j,-n-1}^* - G_{-j,-n+1}^*) + \gamma_2 n_2 \delta_{j,0} \delta_{n,0}, \quad (2.11)$$

$$M_{jn}^3 D_{jn} = -A_b(G_{j,n-1} - G_{j,n+1}) - A_b^*(G_{-j,-n-1}^* - G_{-j,-n+1}^*) + \gamma_3 n_3 \delta_{j,0} \delta_{n,0}, \quad (2.12)$$

$$L_{jn}^a F_{jn} = -A_a^*(C_{j-1,n} - C_{j+1,n} - B_{j-1,n} + B_{j+1,n}) + A_b(S_{j,n-1} - S_{j,n+1}), \quad (2.13)$$

$$L_{jn}^b G_{jn} = -A_b^*(D_{j,n-1} - D_{j,n+1} - C_{j,n-1} + C_{j,n+1}) - A_a(S_{j-1,n} - S_{j+1,n}), \quad (2.14)$$

$$L_{jn}^c S_{jn} = -A_a^*(G_{j-1,n} - G_{j+1,n}) + A_b^*(F_{j,n-1} - F_{j,n+1}). \quad (2.15)$$

It is easily shown that  $F_{1,0}$ ,  $F_{-1,0}$ ,  $G_{0,1}$ , and  $G_{0,-1}$  are the coefficients of the only Fourier terms of the induced polarization having a significant projection onto the cavity modes. Therefore any field amplification or dispersion must come from these terms. Only terms which couple to these terms are of interest. Such terms are

$$B_{jn}, C_{jn}, D_{jn} \text{ for } j, n \text{ even,}$$

$$F_{jn} \text{ for } j \text{ odd and } n \text{ even,}$$

$$G_{jn} \text{ for } j \text{ even and } n \text{ odd,}$$

$$S_{jn} \text{ for } j \text{ odd and } n \text{ odd.}$$

All other terms are zero. The rest of this work involves the solution of Eqs. (2.10) through (2.15), and the application of the self-consistency condition to obtain the intensities and frequencies of the laser modes. These difference equations were first published in our paper announcing some preliminary results of the current investigation.<sup>23</sup>

The macroscopic polarization density in velocity space is obtained from the density matrix

$$\frac{dP}{dv} \equiv \hat{x} P(v, z) = \hat{x} \text{tr}(\mu \rho), \quad (2.16)$$

where  $\mu$  is the atomic dipole operator and  $\rho$  is the density matrix.  $P$  is obtained by averaging the distribution function  $P(v, z)$  over the atomic velocity distribution  $w(v)$ ,

$$P = \hat{x} \int_{-\infty}^{\infty} dv w(v) P(v, z). \quad (2.17)$$

We have chosen to normalize the density matrix such that its trace is the expectation value of the number density of atoms which are in any of the states  $\Psi_1$ ,  $\Psi_2$ , and  $\Psi_3$ .

Equations (2.16) and (2.17) give the macroscopic polarization once Eqs. (2.10)–(2.15) have been solved. The in-quadrature and in-phase components of the source polarization density for mode  $a$  are easily shown to be

$$P_a^q = 2\mu_a \int_{-\infty}^{\infty} dv w(v) \text{Re}(F_{1,0}^0 - F_{-1,0}^0), \quad (2.18)$$

$$P_a^p = 2\mu_a \int_{-\infty}^{\infty} dv w(v) \text{Im}(F_{-1,0}^0 - F_{1,0}^0). \quad (2.19)$$

Similarly, the polarization components which interact with mode  $b$  are found to be

$$P_b^q = 2\mu_b \int_{-\infty}^{\infty} dv w(v) \text{Re}(G_{0,1}^0 - G_{0,-1}^0), \quad (2.20)$$

$$P_b^p = 2\mu_b \int_{-\infty}^{\infty} dv w(v) \text{Im}(G_{0,-1}^0 - G_{0,1}^0), \quad (2.21)$$

where  $F_{\pm 1,0}^0$  and  $G_{0,\pm 1}^0$  are defined in Appendix A. The superscripts indicate that  $F_{\pm 1,0}^0$  and  $G_{0,\pm 1}^0$ , and therefore  $P_a^q$  and  $P_b^p$ , are independent of the phases of  $A_a$  and  $A_b$ . These components of the polarization density are related to the gain and refractive index in the well-known way.<sup>1</sup> Equations

(2.18)–(2.21) relate the Fourier coefficients of (2.10)–(2.15) to the laser gain and refractive index.

Thus, for assumed field amplitudes  $E_a$  and  $E_b$ , we can solve (2.10)–(2.15) numerically to obtain the  $F$ 's and  $G$ 's. We then use the self-consistency conditions for modes  $a$  and  $b$  to obtain the gains, i.e., the gains of the modes must be equal to cavity losses. The method used to satisfy the self-consistency condition is to numerically search for values of  $E_a$  and  $E_b$  for which  $g_a$  and  $g_b$  are equal to the assumed loss per unit length of the laser.

Our numerical approach to the solution of the difference equations (2.10)–(2.15) is described in Appendix A. Further details of the approach are available elsewhere.<sup>27</sup>

It will be useful in what follows to introduce variables for the zero-field population inversions, products of the Rabi frequencies, and other useful quantities:

$$\begin{aligned}\xi_a &= n_2 - n_1, \quad \xi_b = n_3 - n_2, \\ r_a &= A_a^* \xi_a, \quad r_b = A_b^* \xi_b, \\ U_a &= A_a^* A_a, \quad U_b = A_b^* A_b, \quad U_c = A_b A_a^*, \\ 1/P_{kn}^a &= 1/M_{kn}^1 + 1/M_{kn}^2, \\ 1/P_{kn}^b &= 1/M_{kn}^3 + 1/M_{kn}^2.\end{aligned}$$

### III. APPROXIMATIONS IN THE THEORY OF THE TWO-TRANSITION LASER

In the preceding section we developed the basic formalism for the semiclassical theory of the three-level, two-transition gas laser. Because of the readily apparent complexity of these equations, an analytical solution seems hopeless. Our own efforts in this direction were indeed fruitless. This is in stark contrast to the theory of the single-transition laser, where considerable analytical progress has been made.<sup>24</sup>

The complexity of the three-level equations has led to various approximation schemes in the theory of the two-transition laser. In order to place our own exact numerical calculations in context, we devote this section to a discussion of the more common approximations. The comparison of our difference equations with these approximations to them will also provide insight into the ranges of validity of the various approximations. In the next section it will be shown that all these approximations are deficient in one way or another in describing the operation of a two-transition laser.

#### A. The rate-equation approximation

In treating two-level gas laser problems, Lamb and collaborators have shown that important effects are associated with the generation of harmonics of the mode wave numbers in the spatial dependence of the density-matrix elements.<sup>1,3,20</sup> These harmonics are called population pulsations because, in the rest frame of a moving atom, the two resonant traveling waves which comprise a standing-wave laser mode are Doppler shifted in frequency by  $\pm kv$ . Therefore the diagonal density-matrix elements are driven at the difference frequency  $2kv$ . This time dependence is transformed into a spatial dependence in going to the rest frame of the laser mirrors.<sup>24</sup> The rate-equation approximation (REA) consists of the neglect of all spatial dependence of higher than first order in the mode wave numbers. Mode locking cannot be treated in this approximation, and the predicted intensity of modes tuned near line center in a two-level single-mode laser may be too low. The two-level theory, including population pulsations of all orders, was found to include the Lamb dip, but the decrease in intensity as the frequency of the mode was swept toward line center was less pronounced than in the REA. For the case of a laser mode tuned to line center, the velocity distribution of the population inversion was found to have a small bump centered at zero velocity in the Bennett hole,<sup>20</sup> but the intensity versus tuning curve did not exhibit a similar bump at line center. Outside the region of the Lamb dip, however, the REA was shown to be a very good approximation for a single-mode laser.<sup>20</sup>

In treating steady-state, three-level atomic resonance problems, the REA has often been used. In our formalism, the REA consists of setting

$$F_{jn} = G_{jn} = S_{jn} = B_{jn} = C_{jn} = D_{jn} = 0 \quad \text{if } j > 1 \text{ or } n > 1.$$

Therefore, the diagonal density-matrix elements have no spatial dependence in the REA. The difference equations (2.10) through (2.15) are then reduced to ten coupled linear algebraic equations

$$Z_a = \frac{2}{\gamma_a} \text{Re}[A_a(F_1 - F_{-1})] - \frac{2}{\gamma_2} \text{Re}[A_b(G_1 - G_{-1})] + \xi_a, \quad (3.1)$$

$$Z_b = \frac{2}{\gamma_b} \text{Re}[A_b(G_1 - G_{-1})] - \frac{2}{\gamma_2} \text{Re}[A_a(F_1 - F_{-1})] + \xi_b, \quad (3.2)$$

$$L_{\pm 1}^a F_{\pm 1} = \mp A_a Z_a + A_b (S_{\pm 1, -1} - S_{\pm 1, 1}), \quad (3.3)$$

$$L_{\pm 1}^b G_{\pm 1} = \mp A_b Z_b + A_a (S_{1, \pm 1} - S_{-1, \pm 1}), \quad (3.4)$$

$$L_{\pm 1, 1}^c S_{\pm 1, 1} = \mp A_a G_1 + A_b F_{\pm 1}, \quad (3.5)$$

$$L_{\pm 1, -1}^c S_{\pm 1, -1} = \mp A_a G_{-1} - A_b F_{\pm 1}, \quad (3.6)$$

where  $Z_a = C_{0,0} - B_{0,0}$ ,  $Z_b = D_{0,0} - C_{0,0}$ ,  $1/\gamma_a = 1/\gamma_1 + 1/\gamma_2$ , and  $1/\gamma_b = 1/\gamma_3 + 1/\gamma_2$ . The second subscripts of  $L^a$  and  $F$ , as well as the first subscripts of  $L^b$  and of  $G$ , have been suppressed because they are always zero in the REA. This system of equations was solved to obtain the REA results to be presented in the next section. The closed-form Doppler-averaged solution of Eqs. (3.1) through (3.6) is rather complicated. These equations take very little computer time to evaluate numerically, however, while the difference equations (2.10)–(2.15) can be quite time consuming; thus it is worthwhile to use the REA equations whenever they are applicable.

An approximate condition for the validity of the REA can be derived by using a perturbation argument. We assume that we know the  $B$ ,  $C$ ,  $D$ ,  $F_{\pm 1}$ , and  $G_{\pm 1}$  in the REA. We can tell when higher Fourier coefficients become appreciable by examining the coefficients of the terms  $B_{ij}$ ,  $C_{ij}$ ,  $D_{ij}$ , and  $S_{ij}$  on the left-hand sides of Eqs. (2.10)–(2.15). For example, a necessary condition for the population pulsations with the coefficient  $B_{jn}$  to be significant is that  $M_{jn}^l$  be small for portions of the atomic velocity distribution with which one of the modes interacts strongly. Population pulsations will not be driven by  $E_a$  unless

$$|jk_a v + nk_b v| < \gamma_1$$

and  $(3.7)$

$$|\Delta_a \pm k_a v| < \beta_a (1 + I_a/2)^{1/2}$$

for some velocity  $v$ , where the dimensionless intensities of the modes are

$$I_a = 4U_a(\gamma_1 + \gamma_2)/(\gamma_1\gamma_2\beta_a), \quad (3.8)$$

$$I_b = 4U_b(\gamma_2 + \gamma_3)/(\gamma_2\gamma_3\beta_b). \quad (3.9)$$

The expression  $\beta_a(1 + I_a/2)^{1/2}$  is the power-broadened Lorentzian half-width of transition  $a$ . This is the width (HWHM) of the Bennett hole which would be burned into the population inversion distribution by a single-frequency traveling-wave electromagnetic field.

The existence of isolated numbers  $j, n$  for which this condition is satisfied does not necessarily imply the generation of population pulsations. Fourier

coefficients with adjacent indices which are coupled to  $B_{jn}$  must also be large; therefore a chain of  $B$ 's and  $F$ 's, all with appreciable magnitudes, must link  $B_{jn}$  with  $F_{1,0}$  or  $F_{-1,0}$ . This condition requires that  $v$  and  $\Delta$  be small for pulsations to be generated. We substitute  $j=2$  and  $n=0$  to obtain the condition for the generation of the lowest-order population pulsations. We obtain the condition

$$|\Delta_a| < \gamma_1 + \beta_a(1 + I_a/2)^{1/2}. \quad (3.10)$$

Since (3.10) is approximate, we may substitute

$$|\Delta_a| < \beta_a(1 + I_a/2)^{1/2}. \quad (3.11)$$

Similarly,

$$|\Delta_b| < \beta_b(1 + I_b/2)^{1/2} \quad (3.12)$$

to allow the generation of population pulsations with coefficients  $C_{0,2}$  and  $D_{0,2}$ .

The direct coupling of the two transition amplitudes by  $\rho_{31}$  can also cause the density-matrix elements  $\rho_{21}$  and  $\rho_{32}$  to contain harmonics of the wave numbers of the modes. The  $L_{jn}^c$  are small when both modes are tuned near line center and higher-order  $S$ 's are resonant. Indeed, the  $S_{ij}$  terms only generate higher harmonics in the polarization oscillations when the modes are tuned in the region of the Lamb dip, near line center.

To study some of the dominant features of Eqs. (3.1) through (3.6), when the detunings of the modes are much *greater* than their respective linewidths, we may examine a pair of resonant traveling waves and ignore the traveling waves that interact with the opposite side of the atomic velocity distribution. We set  $F_{-1} = G_{-1} = 0$  for the case of copropagating waves or  $F_{-1} = G_1 = 0$  for the counterpropagating case. Then Eqs. (3.1)–(3.6) reduce to

$$Z_a = \frac{2}{\gamma_a} \text{Re}(A_a F) - \frac{2\epsilon}{\gamma_2} \text{Re}(A_b G) + \xi_a, \quad (3.13)$$

$$Z_b = \frac{2\epsilon}{\gamma_b} \text{Re}(A_b G) - \frac{2}{\gamma_2} \text{Re}(A_a F) + \xi_b, \quad (3.14)$$

$$L^a F = -A_a Z_a - \epsilon A_b S, \quad (3.15)$$

$$L^b G = -\epsilon A_b Z_b + A_a S, \quad (3.16)$$

$$L^c S = -A_a G + \epsilon A_b F, \quad (3.17)$$

where  $F = F_1$ ,  $G = G_\epsilon$ ,  $S = S_{1,\epsilon}$ ,  $L^a = L_1^a$ ,  $L^b = L_\epsilon^b$ ,  $L^c = L_{1,\epsilon}^c$ , and  $\epsilon = +1(-1)$  for the copropagating (counterpropagating) case. These equations would have resulted if we had simply substituted traveling-wave fields into the density-matrix equations (2.2) and (2.3) rather than the standing-wave fields. From Eq. (2.18), it is apparent that the gain for mode  $a$  is proportional to  $\text{Re}F$ . For the traveling-wave case, we obtain

$$h \equiv A_a \text{Re} F = [(1+s_a)(1+s_b) - W_a W_b]^{-1} \{ -[\epsilon X W_a + T_a(1+s_b)] \xi_a - [\epsilon T_b W_a + X(1+s_b)] \xi_b \}, \quad (3.18)$$

where

$$\begin{aligned} s_a &= 2T_a/\gamma_a - 2X/\gamma_2, \quad s_b = 2T_b/\gamma_b - 2X/\gamma_2, \\ W_a &= 2\epsilon T_a/\gamma_2 - 2\epsilon X/\gamma_b, \quad W_b = 2\epsilon T_b/\gamma_2 - 2\epsilon X/\gamma_a, \\ T_a &= U_a R_a + U_a^2 R_{abc}, \quad T_b = U_b R_b + U_b^2 R_{abc}, \\ X &= U_a U_b R_{abc}, \quad R_a = \text{Re}(\eta L^a)^{-1}, \\ R_b &= \text{Re}(\eta L^b)^{-1}, \quad R_{abc} = \text{Re}(\eta L^a L^b L^c)^{-1}, \\ \eta &= 1 + U_a/(L^b L^c) + U_b/(L^a L^c), \end{aligned}$$

and the  $U$ 's and  $\xi$ 's are defined in Sec. II. This equation is sufficiently complicated that interpretation is difficult. This is, however, an important equation from which we can derive equations for limiting cases which are more easily interpreted.

An approximate version in which only terms of first order in  $A_a$  are retained<sup>4-6,11-14</sup> has been studied extensively in the literature. This limit corresponds to determining the small-signal gain of transition  $a$ , while a field of arbitrary intensity saturates transition  $b$ . Javan has described the structure which occurs in this case for stationary atoms.<sup>28,29</sup> The desired equation is

$$h = h' \xi_b + h'' \xi_a, \quad (3.19)$$

where

$$h' = -\text{Re} U_a U_b \frac{\left[ L^{b*} + \frac{2L^c \beta_b}{\gamma_2} \right]}{\left[ |L^b|^2 + \frac{2U_b \beta_b}{\gamma_b} \right] (L^a L^c + U_b)}, \quad (3.20a)$$

$$h'' = -\text{Re} \frac{U_a L^c}{L^a L^c + U_b}. \quad (3.20b)$$

The terms in Eq. (3.19) exhibit the dynamic Stark effect; that is, the resonance structure of the atom is changed by the existence of a rapidly varying electric field. To show the effect, we write the second term as the sum of two expressions, each of which contains a resonance as  $\Delta_a$  is varied,

$$h'' = \text{Re} \left[ x \left[ \frac{1}{\Delta'_a + K_+} - \frac{1}{\Delta'_a + K_-} \right] \right], \quad (3.21)$$

where

$$\begin{aligned} K_{\pm} &= \frac{1}{2} (\Delta'_b - i(\beta_a + \beta_c) \\ &\quad \pm \{ [\Delta'_b + i(\beta_a - \beta_c)]^2 + 4U_b \}^{1/2}), \end{aligned}$$

$$x = \frac{U_a L^c}{K_- - K_+},$$

$$\Delta'_a = \Delta_a + k_a v \quad \text{and} \quad \Delta'_b = \Delta_b + \epsilon k_b v.$$

If  $\Delta'_b$  is very large,  $K_+$  is very large, so we may ignore the first term in parenthesis of Eq. (3.21). The second term can then be approximated as

$$h'' \cong -\text{Re} \left[ \frac{x}{\Delta'_a - \frac{U_b}{\Delta'_b} - i\beta_a} \right]. \quad (3.22)$$

The resonance is shifted by an amount  $U_b/\Delta'_b$ . This is the usual quadratic Stark shift of level two due to a rapidly varying field when only one other transition is treated.

For  $\Delta'_b$  small, Eq. (3.21) is the sum of two resonances with their peaks separated by an amount  $\text{Re}[(\Delta'_b + i\beta_a - i\beta_c)^2 + 4U_b]^{1/2}$ . For  $\beta_a$  and  $\beta_c$  small, this splitting is just equal, as one might expect, to the Rabi frequency of transition  $b$ . The Doppler limit averaging of Eq. (3.21) in some cases retains the split resonance, but in other cases this structure will totally disappear.

The denominator of  $h'$  also contains the factor  $L_a L_c + U_b$ , so it also has the form of Eq. (3.21), but with  $X$  replaced by a different constant. We shall see that the velocity averaging of this term will eliminate the splitting for some, but not all, situations. Javan has discussed the structure we have noted regarding Eqs. (3.19) through (3.22).<sup>28,29</sup>

Another important feature of the interaction involves the integral of  $h$  with respect to  $\Delta'_a$ . Javan first showed that this integral is dependent only on the population inversion of transition  $a$ .<sup>29</sup> Its value is unaffected by the direct-coupling effects introduced by the density-matrix element  $\rho_{31}$  when a field is resonant with transition  $b$ . Specifically,

$$\int_{-\infty}^{\infty} d\Delta'_a h = \int_{-\infty}^{\infty} d\Delta'_a U_a Z_a \text{Re} \frac{1}{L_a}. \quad (3.23)$$

Feldman and Feld pointed out that the area (integral with respect to  $\Delta_a$ ) of the gain of a Doppler-broadened gas is also determined by  $Z_a(v)$  alone because Eq. (3.23) holds for any group of atoms with a single velocity.<sup>13</sup> They have also shown that this principle is independent of the form of the saturat-

ing field.<sup>30</sup> It therefore holds for standing waves as well as traveling waves.

The Doppler-limit integral of Eq. (3.19) can be obtained in closed form and represents a limiting case of a three-level laser which is detuned from resonance.<sup>11,13</sup> We shall include these equations because they have a resonance structure similar to that in our numerical results. Equations (3.24)–(3.27) give the result for the low-pressure case  $[\beta_a = \frac{1}{2}(\gamma_1 + \gamma_2), \beta_b = \frac{1}{2}(\gamma_2 + \gamma_3),$  and

$\beta_c = \frac{1}{2}(\gamma_1 + \gamma_3)]$ . This low-pressure case will be emphasized in the numerical results to be presented in the next section. If  $U_b$  is very large, the result differs qualitatively depending on which is larger,  $k_a$  or  $k_b$ . If  $k_a > k_b$ , the solution reduces to a Lorentzian whose width is dependent on whether the beams are copropagating ( $\epsilon = +1$ ) or counterpropagating ( $\epsilon = -1$ ),

$$M'' \equiv \int_{-\infty}^{\infty} dv h_a'' = -\pi U_a / k_a \quad (3.24)$$

$$M' \equiv \int_{-\infty}^{\infty} dv h_a' = \frac{2\pi U_a U_b}{k_b \gamma_2 Y} \operatorname{Re} \left\{ \left[ i \left[ -\Delta_a + \epsilon \frac{k_a}{k_b} \Delta_b \right] - \frac{1}{2} \left[ \gamma_1 + \frac{k_a}{k_b} \gamma_3 + \frac{k_b + \epsilon k_a}{k_b} \gamma_2 \right] \right]^{-1} \right\}, \quad (3.25)$$

where  $Y = (1 - 4U_b / \gamma_2 \gamma_3)^{1/2}$  is the power-broadening coefficient for the homogeneous linewidth of transition  $b$ . These equations also apply if  $\epsilon = +1$  and  $k_a < k_b$ . The resonance of  $M'$  is shifted by  $\epsilon \Delta_b k_a / k_b$  because the group of atoms centered at velocity  $v$  will interact with both laser modes if  $\Delta_a = k_a v$  and  $\epsilon \Delta_b = k_b v$ .

For  $U_b$  large,  $k_b > k_a$ , and  $\epsilon = -1$ , the Doppler average of Eq. (3.19) preserves the splitting of the resonance which occurs for any single velocity group of atoms. In this case

$$M'' = \frac{\pi U_a}{k_a} \operatorname{Im}(\tau / y), \quad (3.26)$$

$$M' = -2\pi U_a U_b k_a / (Y k_b^2) \operatorname{Im}(y^{-1} \{ b_+^{-1} [ \frac{1}{2}(1+Y) + i(k_a - k_b)(a_+ + d) / (\gamma_2 k_a) ] + b_-^{-1} [ \frac{1}{2}(1-Y) + i(k_a - k_b)(a_- + d) / (\gamma_2 k_a) ] \} ), \quad (3.27)$$

where

$$y = (q^2 - \tau^2)^{1/2},$$

with

$$\operatorname{Re} y < 0, \quad q^2 = 4k_a(k_b - k_a)U_b / k_b^2,$$

$$\tau = -\Delta_a - \Delta_b k_a / k_b + \frac{1}{2} i \{ [k_a \gamma_3 + (k_b - k_a) \gamma_2] / k_b + \gamma_1 \},$$

$$a_{\pm} = \frac{1}{2} k_b (\tau \pm iy) / (k_a - k_b) - \Delta_a + i \beta_a,$$

$$b_{\pm} = \pm a_{\pm} + k_a (i \beta_b Y \mp \Delta_b) / k_b,$$

and

$$d = k_a (\Delta_c - i \beta_c) / (k_a - k_b).$$

Equation (3.27) has been shown to correspond to a split resonance with the splitting proportional to  $U_b$ .<sup>13,31</sup> Our calculated results show that this split resonance also occurs when both  $U_a$  and  $U_b$  are appreciable. Equation (3.26) also exhibits a split resonance, even if  $U_b$  is small. For small  $U_b$ , no splitting of  $M'$  occurs and Eq.(3.25) also applies for  $k_b > k_a, \epsilon = -1$ .

## B. Independent-field approximations (IFA)

Under certain circumstances, the direct coupling of the dipole transition density-matrix elements  $\rho_{21}$  and  $\rho_{32}$  by the element  $\rho_{31}$  is negligible. Setting  $\rho_{31} = 0$  is known as the independent-field approximation (IFA). The  $\rho_{31}$  density-matrix element has terms corresponding to the Raman effect, as well as to the splitting of the resonances and to the quadratic Stark effect discussed above. When  $\rho_{31} = 0$ , Eqs. (2.13) and (2.14) are replaced by

$$L_{jn}^a F_{jn} = -A_a (C_{j-1,n} - C_{j+1,n} - B_{j-1,n} + B_{j+1,n}), \quad (3.28)$$

$$L_{jn}^b G_{jn} = -A_b (D_{j,n-1} - D_{j,n+1} - C_{j,n-1} - C_{j,n+1}), \quad (3.29)$$

while Eqs. (2.10)–(2.12) remain unchanged.

We will now derive approximate conditions for the validity of the IFA starting, for simplicity, from the REA traveling-wave equations. Using Eq. (3.17) to eliminate  $S$  from Eqs. (3.15) and (3.16), the

equations for  $h_a$  and  $h_b$  are found to be

$$\begin{aligned} [1 + U_a/(L_b L_c) + U_b/(L_a L_c)] A_a F \\ = -U_a U_b Z_b / (L_a L_b L_c) \\ - [U_a/L_a + U_a^2/(L_a L_b L_c)] Z_a, \end{aligned} \quad (3.30)$$

$$\begin{aligned} [1 + U_b/(L_a L_c) + U_a/(L_b L_c)] A_b G \\ = -U_a U_b Z_a / (L_a L_b L_c) \\ - [U_b/L_b + U_b^2/(L_a L_b L_c)] Z_b. \end{aligned} \quad (3.31)$$

In the IFA these equations reduce to

$$A_a F = -U_a Z_a / L_a, \quad (3.32)$$

$$A_b G = -U_b Z_b / L_b. \quad (3.33)$$

Near resonance,  $L_a \cong \beta_a$ ,  $L_b \cong \beta_b$ , and  $L_c \cong \beta_c$ . Therefore, to ensure that Eqs. (3.32) and (3.33) accurately describe the resonant interaction, the following conditions are necessary:

$$U_a / \beta_b \beta_c \ll 1, \quad (3.34)$$

$$U_b / \beta_a \beta_c \ll 1, \quad (3.35)$$

$$U_a Z_a / \beta_a \beta_c Z_b \ll 1, \quad (3.36)$$

$$U_b Z_b / \beta_b \beta_c Z_a \ll 1. \quad (3.37)$$

If  $\gamma_1$  is not too different from  $\gamma_3$  and  $\xi_a$  is not too different from  $\xi_b$ , then conditions (3.34) and (3.35) imply (3.36) and (3.37). In some lasers with considerable pressure broadening, for typical operating intensities, the IFA is a good approximation because

$$I_a = 4U_a(\gamma_1 + \gamma_2) / \gamma_1 \gamma_2 \beta_a, \quad (3.38)$$

$$I_b = 4U_b(\gamma_2 + \gamma_3) / \gamma_2 \gamma_3 \beta_b. \quad (3.39)$$

Then condition (3.34) may be written

$$I_a \gamma_1 \gamma_2 \beta_a / [4(\gamma_1 + \gamma_2) \beta_b \beta_c] \ll 1. \quad (3.40)$$

If elastic collision broadening predominates over the linewidths determined by the decay of the diagonal density-matrix elements, then  $\beta_1$ ,  $\beta_2$ , and  $\beta_3$  will usually have comparable magnitudes, and their magnitudes may be much larger than any of  $\gamma_1$ ,  $\gamma_2$ , or  $\gamma_3$ .  $I_a$  is the usual dimensionless intensity of the laser and is fixed by the cavity  $Q$  because of the "gain equals loss" condition. The dimensionless intensity is typically between 1 and 30, but it can be much greater. For a moderate value of  $I_a$ , some gases (such as  $\text{CO}_2$  at moderate pressures) satisfy condition (3.40).

It is also apparent from conditions (3.34)–(3.37) that if  $\beta_c$  is large, the IFA may be a good approximation. More specifically, if  $\beta_c \gg U_b / \beta_a$ ,

$\beta_c \gg U_a / \beta_b$ ,  $\beta_c \gg U_b Z_b / \beta_b Z_a$ , and  $\beta_c \gg U_a Z_a / \beta_a Z_b$ , the IFA will give valid results. It may be shown<sup>27</sup> that in the IFA

$$F_{-n,-m} = -L_{n,m}^{a*} F_{n,m}^* / L_{-n,-m}^a \quad (3.41)$$

and

$$G_{-n,-m} = -L_{n,m}^{b*} G_{n,m}^* / L_{-n,-m}^b. \quad (3.42)$$

As a result, the rank of the matrix is decreased by a factor of one half. The terms multiplying the  $F_{ij}$  and  $G_{ij}$  with  $i+j < 0$  combine with other terms, and most rows of the resulting matrix have 14 nonzero real elements. No row has more than that number. The difference equations obtained by eliminating the Fourier coefficients of the diagonal density-matrix elements from Eqs. (2.10)–(2.12) and (3.28) and (3.29) are rather involved and will not be written out here.<sup>27</sup>

The gain of either transition is a symmetric function of the detuning of that transition from line center when the IFA is used, whereas the resonant contribution to the index of refraction is an antisymmetric function,

$$P_a^q(-\Delta_a) = P_a^q(\Delta_a), \quad (3.43)$$

$$P_a^p(-\Delta_a) = -P_a^p(\Delta_a). \quad (3.44)$$

A derivation of these properties is given in Ref. 27. Our calculated gains for the case of negligible elastic-collision broadening compared with the decay rates of the level populations show a significant asymmetry with respect to line center, so the IFA is clearly not a good approximation for these cases.

### C. Simple rate-equation approximation (SREA)

Here, the simple rate-equation approximation (SREA) will refer to the combination of the IFA with the REA. In the literature, our SREA has sometimes been called the REA. Effects due to the burning of Bennett holes in the velocity distributions of the level populations are still present in this approximation, as are cascading effects (i.e., the same atom may undergo successive transitions caused by stimulated emission from level three to level two and from level two to level one). We will show that as a result of cascading, it is possible for lasing to occur on a transition which has no zero-field population inversion.

The SREA has been applied to the He-Ne laser operated as a three-level cascading system by Haken *et al.*<sup>32</sup> In that treatment, decay among the lasing

levels, which we have omitted, was included. Discussions of the three-level resonance problem using the SREA are included in several other publications.<sup>4,6</sup>

As far as we know, the SREA has always been used in computer models of multitransition high-energy lasers, which include detailed molecular kinetics models.<sup>17-19</sup> In fact, additional simplifying assumptions, such as line-center operation and homogeneous saturation of the gain curve, are usually used.

Equations (2.10) through (2.14) reduce to the following set of equations in the SREA:

$$\begin{aligned} Z_a = 2A_a \left[ \frac{1}{\gamma_2} + \frac{1}{\gamma_1} \right] \text{Re}(F_1 - F_{-1}) \\ - \frac{2A_b}{\gamma_2} \text{Re}(G_1 - G_{-1}) + \xi_a, \end{aligned} \quad (3.45)$$

$$\begin{aligned} Z_b = 2A_b \left[ \frac{1}{\gamma_2} + \frac{1}{\gamma_3} \right] \text{Re}(G_1 - G_{-1}) \\ - \frac{2A_a}{\gamma_2} \text{Re}(F_1 - F_{-1}) + \xi_b, \end{aligned} \quad (3.46)$$

$$L_{\pm 1}^a F_{\pm 1} = \mp A_a Z_a, \quad (3.47)$$

$$L_{\pm 1}^b G_{\pm 1} = \mp A_b Z_b. \quad (3.48)$$

Subscripts, which are always zero in the SREA, have been suppressed; for example,  $L_{\pm 1}^a \equiv L_{\pm 1,0}^a$ . Equations (3.45)–(3.48) are almost in the form normally incorporated in engineering computer codes which are used to design high-energy lasers. To put them into that form, we relax the steady-state conditions and write equations for the level populations

$$\dot{\rho}_{11} = -\gamma_1 \rho_{11} + l_{21}(\rho_{22} - \rho_{11}) + r_1, \quad (3.49)$$

$$\begin{aligned} \dot{\rho}_{22} = -\gamma_2 \rho_{22} + l_{32}(\rho_{33} - \rho_{22}) \\ - l_{21}(\rho_{22} - \rho_{11}) + r_2, \end{aligned} \quad (3.50)$$

$$\dot{\rho}_{33} = -\gamma_3 \rho_{33} - l_{32}(\rho_{33} - \rho_{22}) + r_3, \quad (3.51)$$

where the diagonal density-matrix elements  $\rho_{ii}(v)$  are the level populations,  $r_i$  are the level-pumping rates, and the stimulated-emission rates are

$$l_{21} = U_a \text{Re} \left[ \frac{1}{L_1^a} + \frac{1}{L_{-1}^a} \right], \quad (3.52)$$

$$l_{32} = U_b \text{Re} \left[ \frac{1}{L_1^b} + \frac{1}{L_{-1}^b} \right]. \quad (3.53)$$

In engineering codes, the additional assumption

of “velocity equilibrium” is also usually imposed on Eqs. (3.49)–(3.53). If we assume that during lasing the populations maintain Maxwellian velocity distributions, we may set  $\rho_{ii} = N_i w(v)$  and  $r_i = r_i' w(v)$ , where  $w(v) = \exp(-v^2/u^2)/(\pi^{1/2}u)$ . After these substitutions are performed, and the equations are integrated with respect to velocity, the rate equations are found to be

$$\dot{N}_1 = -\gamma_1 N_1 + l'_{21}(N_2 - N_1) + r'_1, \quad (3.54)$$

$$\begin{aligned} \dot{N}_2 = -\gamma_2 N_2 + l'_{32}(N_3 - N_2) \\ - l'_{21}(N_2 - N_1) + r'_2, \end{aligned} \quad (3.55)$$

$$\dot{N}_3 = -\gamma_3 N_3 - l'_{32}(N_3 - N_2) + r'_3, \quad (3.56)$$

where

$$l'_{21} = 2U_a \int_{-\infty}^{\infty} dv w(v) \beta_a / [\beta_a^2 + (\Delta_a + kv)^2], \quad (3.57)$$

$$l'_{32} = 2U_b \int_{-\infty}^{\infty} dv w(v) \beta_b / [\beta_b^2 + (\Delta_b + kv)^2]. \quad (3.58)$$

The integrals  $l'_{21}$  and  $l'_{32}$  are Voigt profiles. Equations (3.54)–(3.58) treat the saturation of the population inversion in an average way rather than allowing different velocity groups of atoms to saturate individually. The velocity equilibrium assumption can cause a drastic overestimation of the power extraction from a Doppler-broadened laser, such as a cascading He-Ne laser with a single mode resonant with each transition. The overall saturation behavior of a Doppler-broadened laser with many longitudinal modes, however, is reasonably well represented by these equations, as is the saturation behavior of a laser which is nearly homogeneously broadened (i.e., a laser with  $\beta$ 's which are on the order of or larger than the  $ku$ 's). Bennett holes are not burned into the velocity distribution for these cases, and the saturation is essentially homogeneous in the sense that most of the velocity groups of atoms have approximately equal population inversions.

In practice, the additional condition  $\Delta_a = \Delta_b = 0$  is frequently imposed on Eqs. (3.54)–(3.58) in laser design analyses.

Returning to the more general rate equations (3.45)–(3.48), we are ultimately interested in calculating  $P_a^q$ ,  $P_b^q$ ,  $P_a^p$ , and  $P_b^p$ . We define

$$F_- = F_1 - F_{-1}, \quad (3.59)$$

$$G_- = G_1 - G_{-1}. \quad (3.60)$$

After substituting these expressions into Eqs.

(3.45)–(3.48) and solving for  $F_-$ , we obtain

$$\operatorname{Re}F_- = -\frac{A_a S_a \gamma_a \left[ \xi_a + \frac{2U_b S_b \gamma_b \xi_b}{\gamma_2(1+2S_b U_b)} \right]}{1+2S_a U_a \left[ 1 - \frac{2\gamma_a \gamma_b U_b S_b}{\gamma_2^2(1+2S_b U_b)} \right]}, \quad (3.61)$$

$$\operatorname{Im}F_- = \frac{\Delta_a [\beta_a^2 + \Delta_a^2 - (k_a v)^2]}{\beta_a [\beta_a^2 + \Delta_a^2 + (k_a v)^2]} \operatorname{Re}F_-, \quad (3.62)$$

$$\gamma_a = \frac{\gamma_2 \gamma_1}{\gamma_2 + \gamma_1}, \quad \gamma_b = \frac{\gamma_3 \gamma_2}{\gamma_3 + \gamma_2}, \quad (3.63)$$

$$S_a = \frac{1}{\gamma_a} \operatorname{Re} \left[ \frac{1}{L_{+1}^a} + \frac{1}{L_{-1}^a} \right],$$

and

$$S_b = \frac{1}{\gamma_b} \operatorname{Re} \left[ \frac{1}{L_{+1}^b} + \frac{1}{L_{-1}^b} \right]. \quad (3.64)$$

Equations for  $G$  can be obtained simply by noting certain symmetry properties which hold when indices are interchanged.<sup>27</sup> The corresponding equation for a two-level atom is obtained by setting  $A_b = 0$  in Eq. (3.61),

$$\operatorname{Re}F_- = -\frac{A_a S_a \gamma_a \xi_a}{1+2S_a U_a}. \quad (3.65)$$

The third level increases the effective zero-field population inversion by the amount of the second term in the brackets in the numerator of Eq. (3.61). In fact, lasing can occur on transition  $a$  even if the zero-field population inversion  $\xi_a$  is negative provided that lasing on the  $b$  transition is adequate to cause

$$\int_{-\infty}^{\infty} dv w(v) \operatorname{Re}F_-(v) > 0. \quad (3.66)$$

Lasing on transition  $b$  increases the population of level two, thus increasing the population inversion of transition  $a$ .

In addition, the saturation is decreased by the second term in brackets in the denominator. For some values of the level decay rates, the gain saturates much more slowly when there is strong lasing on the coupled transition. Suppose that near resonance  $S_b A_b^2 \gg 1$ . Also let  $\gamma_1 \gg \gamma_2$  and  $\gamma_3 \gg \gamma_2$ . Then the term in brackets in the denominator in (3.61) is

$$1 - \frac{2\gamma_a \gamma_b U_b S_b}{\gamma_2^2(1+2S_b U_b)} \cong \frac{\gamma_2}{\gamma_1} + \frac{\gamma_2}{\gamma_3} \ll 1. \quad (3.67)$$

This large decrease in saturation is caused by the lasing on transition  $b$  feeding the population of level two. Level two is only being pumped at a rate  $n_2 \gamma_2$ , which is slow because  $\gamma_2$  is small. Similarly, lasing on transition  $a$  increases lasing on transition  $b$  by preventing the formation of a bottleneck due to the slow decay rate of level two. When the effective saturation is decreased due to cascading, the power broadening is likewise diminished.

#### IV. CALCULATED RESULTS

Numerical solutions of the exact density-matrix equations (2.10)–(2.15) were obtained by using a sparse-matrix method.<sup>33</sup> The general computational strategy is described in Appendix A.

As a first step in testing our computer code, we verified that certain symmetry properties<sup>27</sup> were displayed. These symmetry properties allowed the velocity integration range to effectively be cut in half.

We then reproduced known results for a high-intensity, single-transition (two-level) laser. We compared intensity versus tuning graphs for the case of strong saturation of the upper transition and insignificant saturation of the lower transition with the results presented in Ref. 24. There was no perceptible difference between our graphs and those of Ref. 24. The code has also been shown to produce the same behavior at large detuning and at low intensity as the REA calculations.

As a final more stringent test of our computer code, we used another method to obtain the small-signal value of  $P_a^q(v)$  for cases with significant saturation of the gain of the upper transition. We used the continued-fraction algorithm of Feldman and Feld to calculate the polarization  $P_a^{qt}(v)$ , induced by a small-signal traveling wave resonant with the lower transition, while a standing wave of arbitrary intensity saturated the upper transition.<sup>13</sup> The in-quadrature component of the polarization, corresponding to a small-signal standing wave resonant with the lower transition, was given by

$$P_a^q(v) = P_a^{qt}(v) + P_a^{qt}(-v). \quad (4.1)$$

Tables I and II show values obtained using the two methods. Agreement to three significant digits was obtained using the two methods for all the trial cases for which  $\kappa$  in Eq. (A10) was less than  $10^{-3}$ . The first two cases, for which agreement is poor, had  $\kappa = 0.01$  and  $\kappa = 0.18$ .

We have thus obtained excellent agreement with earlier three-level resonance calculations. These

TABLE I. Normalized values for  $P_a^q(v)$  calculated using our difference equations and the continued-fraction method of Feldman and Feld. A low-intensity standing-wave mode was resonant with transition  $a$ . The following parameters were the same for all cases:  $\gamma_1=1.90$ ,  $\gamma_2=0.50$ ,  $\gamma_3=0.10$ ,  $\beta_a=1.20$ ,  $\beta_b=0.30$ ,  $\beta_c=1.00$ ,  $\xi_a=0.0$ . The  $\gamma$ 's,  $\Delta$ 's,  $\beta$ 's,  $k_a v$ ,  $k_b v$ , and  $U_b^{1/2}$  are normalized; only their relative values affect the results.

$k_a$	$k_b$	$\Delta_a$	$\Delta_b$	$U_b$	$l$	$v$	$\kappa$	$-P_a^q(v)$ Difference equations	$-P_a^q(v)$ Continued fraction
1.90	3.80	1.00	0.500	8.00	13	0.100	0.011	0.0330	0.0377
1.90	3.80	1.00	0.500	5.00	13	0.100	0.182	0.0506	0.0485
1.90	3.80	1.00	0.500	1.00	13	0.100	$7 \times 10^{-4}$	0.0964	0.0963
1.90	3.80	1.00	0.500	0.500	13	0.100	$5 \times 10^{-6}$	0.1013	0.1012
1.90	3.80	-1.00	0.500	1.00	5	1.30	$1 \times 10^{-5}$	0.00995	0.00995
1.90	3.80	1.00	0.500	1.00	5	1.30	$1 \times 10^{-5}$	0.01609	0.01609
1.90	3.80	-1.00	0.500	1.00	7	0.300	$9 \times 10^{-5}$	0.07803	0.07803
1.90	3.80	1.00	0.500	1.00	9	0.300	$1 \times 10^{-6}$	0.08099	0.08099
3.80	1.90	-1.00	0.500	1.00	7	0.700	$3 \times 10^{-5}$	0.3716	0.3716
3.80	1.90	1.00	0.500	1.00	7	0.700	$2 \times 10^{-5}$	0.3607	0.3607

checks have also served the purpose of providing experience in the tolerances needed to obtain a converged solution as defined above.

To study graphs of the mode intensities as a function of the gain and detunings, we have generated numerical results corresponding to typical parameters rather than fitting them to a specific

gain medium. The results shown in Figs. 4 and 5 correspond to the following conditions:

$$\begin{aligned} \gamma_1=1.9, \quad \gamma_2=1.9, \quad \gamma_3=1.0, \quad \beta_a=1.9, \\ \beta_b=1.45, \quad \beta_c=1.45, \quad k_a u=72.2, \\ k_b u=36.1, \quad \frac{\mu_a^2}{\mu_b^2}=1.11, \quad \frac{\xi_a}{\xi_b}=1.18, \end{aligned}$$

TABLE II. Normalized values for  $P_a^q(v)$  calculated using our difference equations and the continued-fraction method of Feldman and Feld. A low-intensity standing-wave mode was resonant with transition  $a$ . The following parameters were the same for all cases:  $\gamma_1=0.90$ ,  $\gamma_2=0.50$ ,  $\gamma_3=2.10$ ,  $\beta_a=0.70$ ,  $\beta_b=1.30$ ,  $\beta_c=1.50$ ,  $\xi_a=0.0$ . The  $\gamma$ 's,  $\Delta$ 's,  $\beta$ 's,  $k_a v$ ,  $k_b v$ , and  $U_b^{1/2}$  are normalized; only their relative values affect the results.

$k_a$	$k_b$	$\Delta_a$	$\Delta_b$	$U_b$	$l$	$v$	$\kappa$	$-P_a^q(v)$ Difference equations	$-P_a^q(v)$ Continued fraction
3.80	1.90	1.00	0.500	0.200	5	0.700	$6 \times 10^{-5}$	0.1482	0.1482
3.80	1.90	-1.00	0.500	2.00	9	0.700	$2 \times 10^{-6}$	0.5093	0.5092
3.80	1.90	1.00	0.500	2.00	9	0.700	$3 \times 10^{-6}$	0.4447	0.4446
1.90	3.80	-1.00	0.500	2.00	5	1.30	$3 \times 10^{-5}$	0.1039	0.1039
1.90	3.80	1.00	0.500	2.00	5	1.30	$3 \times 10^{-5}$	0.1194	0.1194
1.90	3.80	1.00	0.500	2.00	7	0.700	$3 \times 10^{-7}$	0.4336	0.4335
1.90	3.80	-1.00	0.500	2.00	7	0.700	$1 \times 10^{-7}$	0.3759	0.3759
1.90	3.80	-1.00	0.500	1.00	5	1.30	$3 \times 10^{-6}$	0.06476	0.06476
1.90	3.80	1.00	0.500	1.00	5	1.30	$3 \times 10^{-6}$	0.07096	0.07095
1.90	3.80	-1.00	0.500	1.00	5	0.700	$3 \times 10^{-6}$	0.3544	0.3544
1.90	3.80	1.00	0.500	1.00	5	0.700	$2 \times 10^{-5}$	0.3901	0.3901
1.90	3.80	1.00	0.500	4.00	7	0.700	$2 \times 10^{-5}$	0.3651	0.3652
1.90	3.80	-1.00	0.500	4.00	7	0.700	$1 \times 10^{-5}$	0.3116	0.3117
1.90	3.30	1.20	0.700	4.00	7	0.700	$7 \times 10^{-5}$	0.2872	0.2873
1.90	3.30	-1.20	0.700	4.00	7	0.700	$6 \times 10^{-5}$	0.2854	0.2855
3.30	1.90	1.20	0.700	2.00	9	0.700	$4 \times 10^{-6}$	0.3999	0.4000
3.30	1.90	-1.20	0.700	2.00	7	0.700	$2 \times 10^{-4}$	0.5281	0.5282

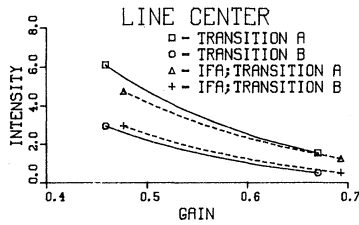


FIG. 4. Intensity versus gain for a three-level cascading laser  $\omega_{21} - \nu_a = 0$ ,  $\omega_{32} - \nu_b = 0$ . Comparison between IFA and difference-equation solutions.

where the  $\gamma$ 's,  $\beta$ 's, and  $ku$ 's have been normalized with respect to  $\gamma_3$ . These parameters correspond to a case of Doppler broadening (i.e., FWHM Doppler widths  $2\sqrt{\ln 2}k_a u$  and  $2\sqrt{\ln 2}k_b u \gg B_a, B_b$ ). The integrations over the zero-field velocity distributions of the populations would then yield Voigt line shapes that for practical purposes would just be Doppler distributions. During lasing, however, the Voigt profiles of the level populations are modified by hole burning in the velocity distribution, and the intensity versus tuning behavior of the laser is also modified by coherence effects resulting from the  $\rho_{31}$  density-matrix element. Additional gain versus intensity curves may be found in Refs. 23 and 27.

In our approach the density-matrix equations have been solved by first prescribing the laser mode intensities, and then the gains have been determined. It was not possible to invert the equations and solve for the intensities in terms of the gains. The condition for steady-state operation, that the gain must balance the loss, determines the intensities in a laser. We have assumed in our calculations that the two modes have the same loss and therefore the same gain. The Newton-Raphson method was used to obtain the same gain at both transition frequencies.  $A_a$  was varied while  $A_b$  was held constant until the relative separation between the gains was less than 0.3%. The plots show the dimensionless

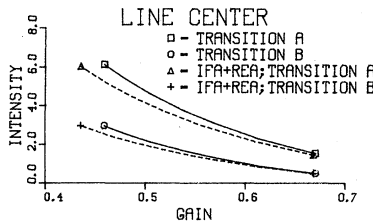


FIG. 5. Intensity versus gain for a three-level cascading laser  $\omega_{21} - \nu_a = 0$ ,  $\omega_{32} - \nu_b = 0$ . Comparison between SREA and difference-equation solutions.

intensities,  $I_a = 4A_a^2(1/\gamma_1 + 1/\gamma_2)/\beta_a$  and  $I_b = 4A_b^2(1/\gamma_2 + 1/\gamma_3)/\beta_b$ , as a function of the normalized gain. That is, the gain at each frequency is plotted in units of  $g_0 = 4\mu_a^2 \pi^{3/2} \xi_a / (\hbar u)$ , the Doppler-limit, line-center, small-signal gain of the lower transition. It has become conventional in laser theory to work with dimensionless intensities as defined here.

Figures 4 and 5 show line-center results; i.e., each mode is exactly resonant with the center frequency of the corresponding transition. At each velocity, the order  $K$  of the Fourier coefficients at which the matrix equation was truncated was selected so that the maximum relative change of either  $g_a$  or  $g_b$  was less than  $10^{-3}$  in going from order  $K-2$  to order  $K$ . This required a maximum of  $K=11$  for the case shown in Figs. 4 and 5. In calculating the density-matrix elements over the range of the velocity distribution for fixed values of  $I_a$  and  $I_b$ , the order  $K$  required for convergence generally fell off as the velocity increased. This monotonic behavior did not always hold very near line center, however, where there was sometimes a small dip in  $K$ . Decreasing the gain and thereby increasing  $I_a$  and  $I_b$  always increased the number of terms required for convergence. For example, for a gain of 0.45, a maximum of  $K=11$  was required for the calculation of Figs. 4 and 5, whereas for a gain of 0.55, a maximum of  $K=9$  was sufficient.

References 4–8 and 11–14 describe the rich structure in the line shape of one transition of a three-level gas when the coupled transition is saturated. Some of these features were discussed in Sec. III. An analogous structure occurs in the self-consistent intensity of one mode if its frequency is varied, while the frequency of the other mode is kept constant. Experimentally, the detuning of the two modes can be varied independently by splitting the two modes with a prism at one end of the laser medium and individually adjusting their path lengths.<sup>15,16</sup> To calculate the self-consistent intensities for a fixed value of the gain, a two-dimensional generalization of the Newton-Raphson method of successive approximation was used. This method is described in Appendix B.

To examine the tuning behavior when both modes were well separated from line center, we used the REA equations (3.1)–(3.6). In this case, the REA is a good approximation.

In the following calculations, the variable  $g$  is defined to be the gain in units of  $g'_0 = 4\mu_b^2 \pi^{3/2} \xi_b / (\hbar u)$ , the Doppler-limit, line-center, small-signal gain of the upper transition.

Figures 6 through 9 illustrate the tuning behavior

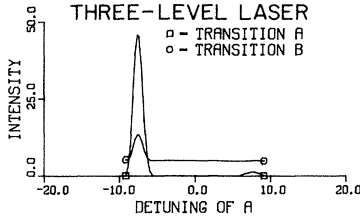


FIG. 6. Three-level cascading laser.  $\gamma_1=0.50$ ,  $\beta_a=\beta_c=0.75$ ,  $\gamma_2=\gamma_3=\beta_b=1.0$ ,  $k_a u=k_b u=30$ ,  $\xi_a=0.0$ ,  $\xi_b=1.0$ ,  $\Delta_b=7.5$ ,  $g=0.47$ ,  $\mu_a^2/\mu_b^2=2.94$ .

of mode  $a$  for  $k_a \geq k_b$  when mode  $b$  is well separated from line center. The zero-field population inversion is zero for transition  $a$ . Therefore no lasing can occur on transition  $a$  unless mode  $b$  is sufficiently strong to increase the gain enough to be above threshold over part of the tuning range. A high, narrow peak occurs on the side of line center opposite that on which mode  $b$  is lasing. A lower, broader peak occurs when modes  $a$  and  $b$  are lasing on the same side of line center. This is similar to the structure which exists in the small-signal gain of transition  $a$  when a strong standing-wave field is resonant with transition  $b$ . As the saturated gain is decreased (by increasing the cavity  $Q$ 's), the intensity of modes  $a$  and  $b$  increases, and mode  $a$  is above threshold over a larger tuning range. Both of the resonances are power broadened increasingly as the intensities increase. Figures 6 through 8 correspond to atoms with the same linewidth parameters and transition frequencies. The detuning of mode  $b$  is also the same for all three plots. The gain is lowered from Fig. 6 to Fig. 7 to Fig. 8, and the intensity of the modes increases in that order. The intensity peaks are broadened as the intensity increases.

Figure 9 corresponds to the case  $k_a=2k_b$ . The intensity peak of mode  $a$  above line center (copropagating case) is very broad. This can be under-

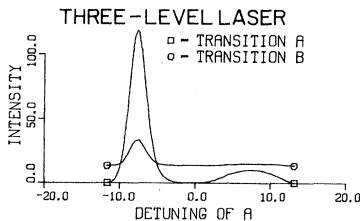


FIG. 7. Three-level cascading laser. Same as Fig. 6 except  $g=0.29$ .

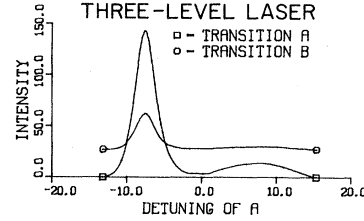


FIG. 8. Three-level cascading laser. Same as Fig. 6 except  $g=0.20$  and  $\mu_a^2/\mu_b^2=2.0$ .

stood by considering the frequency interval  $\Delta\nu_a$ , over which mode  $a$  interacts strongly with atoms which also interact strongly with mode  $b$ . The velocity interval of atoms interacting strongly with mode  $b$  is  $\Delta v = \Delta\nu_b/k_b$ . But since  $\Delta\nu_a = k_a \Delta\nu_b$ ,  $\Delta\nu_a = k_a \Delta\nu_b/k_b$  is the frequency interval over which an increase in the intensity of mode  $a$  is to be expected. The half-width of  $\nu_b$  is  $\Delta\nu_b = \gamma_b(1+I/2)^{1/2}$ , or  $\Delta\nu_b \cong 5\gamma_b = 5$ . Therefore the half-width of  $\nu_a$  is 10. The narrower peak below line center is dominated by Raman-type resonance terms involving denominators of the form  $\{i[\Delta_a + \Delta_b + (k_a - k_b)v] + \beta_c\}^{-1}$ , so this simple argument is not applicable to it. The partial cancellation of the Doppler frequency shifts increases the velocity interval of strongly interacting atoms when  $\Delta_a \cong k_a \Delta_b/k_b$ , so that the direct coupling of the transition amplitudes by the  $\rho_{31}$  density-matrix element introduces significant structure.

The case  $k_a < k_b$  is illustrated by Figs. 10 through 13. The resonance below line center (counter-propagating case) is split, as one would expect by analogy to the case for the small-signal limit of mode  $a$ . This is not surprising because in the Doppler limit, one can obtain the zero crossings of mode  $a$  using Eqs. (3.24) through (3.27). Our numerical solutions are not Doppler-limit cases, because we found it convenient to use fairly narrow Doppler widths to conserve computer time. The

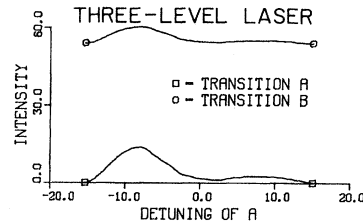


FIG. 9. Three-level cascading laser. Same as Fig. 6 except  $g=0.12$ ,  $k_a u=60$ ,  $k_b u=30$ ,  $\Delta_b=3.75$ , and  $\mu_a^2/\mu_b^2=0.40$ .

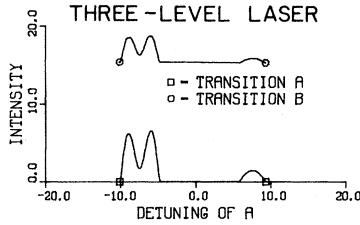


FIG. 10. Three-level cascading laser.  $\gamma_1=0.5$ ,  $\gamma_2=\gamma_3=\beta_b=1.0$ ,  $\beta_a=\beta_c=0.75$ ,  $k_a u=30$ ,  $k_b u=60$ ,  $\xi_a=0.0$ ,  $\xi_b=1.0$ ,  $\Delta_b=15$ ,  $g=0.3$ ,  $\mu_a^2/\mu_b^2=2.0$ .

very slow fall-off of a Lorentzian resonance requires a very large integration range to perform a Doppler-limit integral numerically. The Maxwell velocity distribution can be selected so that its HWHM is much broader than the Lorentzian FWHM, but it still provides a cutoff for the numerical integration.

The splitting of the resonances of Figs. 10 through 13 increases and the two intensity bumps of mode  $a$  are increasingly power broadened as the intensities of modes  $a$  and  $b$  increase. Figure 13 illustrates a case for which the double peaked resonance is not well separated because mode  $b$  is closer to line center and has higher intensity. The higher intensity of mode  $a$  due to the higher intensity of mode  $b$  and due to its larger dipole moment also power broadens the peaks of the split resonance more than in Fig. 10. This plot contains some error in the region  $-2 < \Delta_a < 2$  because the REA was used to generate it. The intensity of mode  $a$  is appreciable in this region so population pulsations should be treated.

The intensity peaks above line center in Figs. 10 through 13 are not split and are similar to the case for  $k_b \leq k_a$ . They are narrower than those of Figs. 6 through 9 because  $k_a < k_b$ . Therefore a frequency interval of mode  $b$  interacts with a velocity interval of atoms which interact with a smaller frequency interval of mode  $a$ , as discussed above.

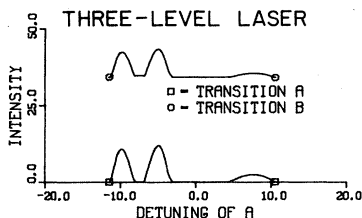


FIG. 11. Three-level cascading laser. Same as Fig. 10 except  $g=0.2$  and  $\mu_a^2/\mu_b^2=1.33$ .

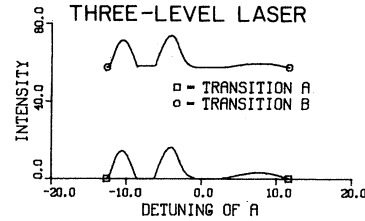


FIG. 12. Three-level cascading laser. Same as Fig. 10 except  $g=0.15$  and  $\mu_a^2/\mu_b^2=1.0$ .

The full difference equation solution is compared with the REA solution in Fig. 14. *The REA plot shows appreciable error.* This will be the case whenever at least one of the modes is tuned within its power-broadened line width [ $\Delta < (1+I/2)^{1/2}$ ] of line center.

All of Figs. 6 through 14 show a strong asymmetry in the detuning of mode  $a$ . The IFA will produce symmetric intensity distributions as a function of the detuning of one of the modes,<sup>27</sup> and therefore it is clear that the IFA, and therefore the SREA, are poor approximations for the range of parameters represented by these results. Figures 4 and 5, Figs. 7 through 10, and Figs. 4 and 5 of Ref. 23 correspond to cases with nonzero small-signal gain resonant with both transitions, and both IFA results and exact results are plotted. The IFA curves are in error, particularly when the detunings of the two modes have opposite signs (counter-propagating case), so the IFA also fails if both transitions have nonzero small-signal gain.

In Figs. 4 and 5, we see that the IFA and the SREA are also in error in predicting line-center intensity versus gain curves. The two approximations lead to different results because population pulsations are significant at line center. The failure of the IFA is the result of our selection of  $\beta$ 's, which are about the same size as the  $\gamma$ 's in performing our calculations. Conditions for the validity of the IFA

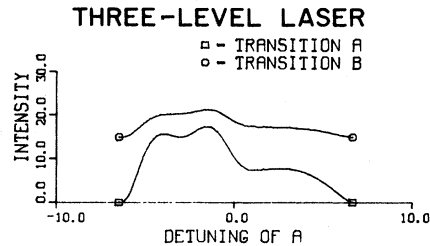


FIG. 13. Three-level cascading laser. Same as Fig. 10 except  $\Delta_b=6.0$ ,  $g=0.3$ , and  $\mu_a^2/\mu_b^2=3.0$ .

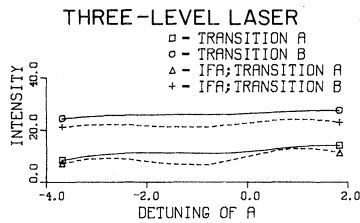


FIG. 14. Three-level cascading laser. Comparison of full difference-equation solutions with REA solutions,  $\gamma_1=0.5$ ,  $\gamma_2=\gamma_3=\beta_b=1.0$ ,  $\beta_a=\beta_c=0.75$ ,  $k_a u=9$ ,  $k_b u=15.35$ ,  $\xi_a=0.0$ ,  $\xi_b=1.0$ ,  $\Delta_b=1.0$ ,  $g=0.18$ ,  $\mu_a^2/\mu_b^2=1.79$ .

are given in Eqs. (3.34) through (3.37), and for  $\beta_c$  very large, or for all the  $\beta$ 's much greater than the  $\gamma$ 's the IFA would be a good approximation and the intensity distributions would be symmetric. For cases with large detunings, such as Figs. 5 through 8, the IFA and the SREA lead to identical curves.

The REA leads to significant error if at least one of the modes is tuned near line center, as is seen in Fig. 14. The REA and exact equations lead to identical results, however, for large detunings of both modes from line center.

The computer time required for a calculation differs greatly, depending on which approximation is used. For example, the amounts of central processor time on a CDC Cyber 176 required to make the calculations for Figs. 4 and 5, and the time to perform the same calculations in the REA were

SREA 2.5 sec ,  
 REA 3.0 sec ,  
 IFA 138 sec ,  
 Exact 842 sec .

## V. CONCLUDING REMARKS

We have described a theory of a laser operating simultaneously on two coupled transitions. Unlike all previous approaches to this type of laser, our theory is accurate for arbitrary mode intensities and detunings. As discussed below, there exist lasers for which our assumptions are not very restrictive.

Previously reported work on the three-level, two-transition laser has all involved approximations to our theory, some of which have been discussed above within the context of our approach. Our new

set of difference equations, which includes the effects of population pulsations and the direct coupling of the two dipole transitions by the  $\rho_{31}$  density-matrix element, were shown to reduce to the REA and IFA equations in limiting cases. Thus it has been possible to compare the predictions of the common approximate approaches with those of our more exact theory. One of our major conclusions from this work is that the two primary approximations, namely the rate-equation approximation (REA) and the independent-field approximation (IFA), can lead to significant errors in the calculation of the output intensities of a laser.

The truncated infinite-dimensional sparse-matrix method used to solve our new difference equations was checked with known results for limiting cases. In the limiting case in which one mode has low intensity while the other is intense enough to saturate its transition, our results are in excellent agreement with the well-known continued-fraction method for solving the density-matrix equations. We have presented some graphs illustrating some of the structure which occurs in the intensity of the modes as a function of the detuning of one of them. This structure is in agreement with all known results for limiting cases. For cases which could not be solved another way, our calculations appeared to converge to unique, reasonable answers.

As has been the case in most "exact" laser theories, we have been mainly interested in the general features of the laser, without focusing on any particular laser system. We do, however, wish to emphasize that real two-transition lasers can be well approximated by our model. Such a laser of current interest is the two-color He-Ne laser, which can be made to operate in a three-level, two-transition mode of the type considered here. Some remarks concerning this system are in order.

Figure 15 is an energy-level diagram for Ne. We show only the dominant transitions responsible for lasing in the infrared and visible. In the cascading laser of Schlemmer *et al.*<sup>15,16</sup> the levels  $2s_2$ ,  $3p_4$ , and  $3s_2$  correspond to our levels 1, 2, and 3, respectively; that is, lasing was observed simultaneously on the two wavelengths  $3.391 \mu\text{m}$  and  $2.395 \mu\text{m}$ . At very low pressures, the  $3s_2$  and the  $2s_2$  levels have short radiative lifetimes, of the order of  $10\text{--}20 \text{ nsec}$ ,<sup>34</sup> due to the strong allowed transitions in the ultraviolet to the ground level. But for neon pressures of about 0.1 Torr, typical of He-Ne lasers, there is considerable radiative trapping of the fluorescent radiation, effectively increasing the lifetimes to  $\tau(2s_2)=0.96 \times 10^{-7} \text{ sec}$  ( $\gamma_1=1.04 \times 10^7 \text{ sec}^{-1}$ ) and  $\tau(3s_2)=1.1 \times 10^{-7} \text{ sec}$  ( $\gamma_3=9.09 \times 10^6$

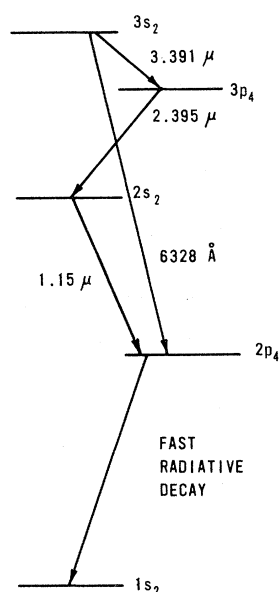


FIG. 15. Energy-level diagram for Ne.

$\text{sec}^{-1}$ ).<sup>35</sup> On the other hand, the lifetime of the  $3p_4$  level is on the order of  $10^{-8}$  sec; this level is not connected to the ground level by an allowed transition, and consequently is not radiatively trapped. The unfavorable lifetime ratio for lasing on the  $2.395 \mu\text{m}$  transition was circumvented by Schlemmer *et al.*<sup>15,16</sup> by broadband lasing on the  $1.15 \mu\text{m}$  transition, which effectively decreased  $\tau(2s_2)$ .

For an effective gas temperature of 400 K, the FWHM Doppler widths are  $\delta\nu_D(3.391 \mu\text{m})=288$  MHz and  $\delta\nu_D(2.395 \mu\text{m})=400$  MHz. With  $\gamma_1$  normalized to unity, therefore, we have

$$\gamma_3=0.87, \quad \gamma_2=10, \quad k_a u=145,$$

and

$$k_b u=104,$$

where we have not included the contribution to  $\gamma_1$  due to the broadband lasing on the  $1.15 \mu\text{m}$  transition. This would decrease the normalized  $\gamma$ 's and  $ku$ 's by a ratio  $\gamma_1/(\gamma_1+\gamma'_1)$ , where  $\gamma'_1$  is the stimulated emission rate. Schlemmer *et al.* did not report the intensity of the lasing on the  $1.15 \mu\text{m}$  transition, but it is clear that the assumption  $k_a u$ ,

$k_b u \gg \gamma_1, \gamma_2, \gamma_3$  made throughout our calculations should be satisfied if  $\gamma'_1$  is not as large as about  $10^9 \text{sec}^{-1}$ . If the stimulated emission rate is in fact that high, our theory is of course still applicable, but the sample calculations presented in the last chapter would not.

If we assume that radiative trapping of the  $2s_2$  and  $3s_2$  levels is fully effective in reducing the natural radiative linewidths of transitions connected to these levels, then  $\beta_a = \frac{1}{2}(\gamma_1 + \gamma_2) = 55$  MHz,  $\beta_b = 55$  MHz, and  $\beta_c = 9.8$  MHz, omitting again the contribution of stimulated emission on the  $1.15 \mu\text{m}$  line to  $\gamma_1$ . The values normalized with respect to  $\gamma_1$  are

$$\beta_a = 5.3, \quad \beta_b = 5.3, \quad \text{and} \quad \beta_c = 0.94,$$

which are also consistent with the sorts of numbers used in our calculations.

Our calculated results show the same general structure as the He-Ne experimental results published in Refs. 15 and 16. We have not performed a detailed comparison with these data, however, because we do not know to what extent the radiative trapping in the laser affected the homogeneous line widths  $\beta_a$ ,  $\beta_b$ , and  $\beta_c$ . To obtain an accurate comparison, a detailed treatment of the radiative trapping would be necessary.

#### ACKNOWLEDGMENTS

We wish to thank S. Swain and E. A. Oliver for useful discussions concerning the difference equations encountered in this work. We also thank C. Chandler for a number of helpful comments, R. Salomaa for providing us with an unpublished copy of Ref. 14, and M. Sargent III for bringing some earlier work to our attention. Research at the University of Arkansas was partially supported by dual funding from NSF EPSCOR Grant No. ISP 8011447 and the State of Arkansas.

#### APPENDIX A: COMPUTATIONAL STRATEGY

It is convenient for the solution of (2.10)–(2.15) to eliminate all the Fourier coefficients except the  $F_{jn}$  and  $G_{jn}$ . We obtain

$$\begin{aligned}
 & Y_{jn}^{jn} F_{jn} + Y_{jn}^{j+2,n} F_{j+2,n} + Y_{jn}^{j-2,n} F_{j-2,n} + Y_{jn}^{j,n+2} F_{j,n+2} + Y_{jn}^{j,n-2} F_{j,n-2} + Y_{jn}^{-1,n-1} G_{j-1,n-1} + Y_{jn}^{j-1,n+1} G_{j-1,n+1} \\
 & + Y_{jn}^{j+1,n+1} G_{j+1,n+1} + Y_{jn}^{j+1,n-1} G_{j+1,n-1} + X_{jn}^{-j,-n} F_{-j,-n}^* + X_{jn}^{-j+2,-n} F_{-j+2,-n}^* + X_{jn}^{-j-2,-n} F_{-j-2,-n}^* \\
 & + X_{jn}^{-j+1,-n+1} G_{-j+1,-n+1}^* + X_{jn}^{-j+1,-n-1} G_{-j+1,-n-1}^* + X_{jn}^{-j-1,-n-1} G_{-j-1,-n-1}^* \\
 & + X_{jn}^{-j-1,-n+1} G_{-j-1,-n+1}^* \\
 & + r_a (\delta_{j,1} - \delta_{j,-1}) \delta_{n,0} = 0.
 \end{aligned} \tag{A1}$$

As noted following Eqs. (2.10)–(2.15), these Fourier coefficients have nonzero values only for  $j$  odd and  $n$  even. Other terms do not couple to  $F_{\pm 1,0}, G_{0,\pm 1}$ , nor to any inhomogeneous driving term ( $r_a$  or  $r_b$ ). For  $j$  odd and  $n$  even, the following definitions have been used:

$$\begin{aligned}
 Y_{j,n}^{j,n} &= L_{j,n}^a + U_a \left[ \frac{1}{P_{j+1,n}^a} + \frac{1}{P_{j-1,n}^a} \right] + U_b \left[ \frac{1}{L_{j,n-1}^c} + \frac{1}{L_{j,n+1}^c} \right], \\
 Y_{j,n}^{j\pm 2,n} &= -U_a / P_{j\pm 1,n}^a, \\
 Y_{j,n}^{j,n\pm 2} &= -U_b / L_{j,n\pm 1}^c, \\
 Y_{j,n}^{j+1,n\pm 1} &= \pm U_c \left[ \frac{1}{M_{j+1,n}^2} + \frac{1}{L_{j,n\pm 1}^c} \right], \\
 Y_{j,n}^{j-1,n\pm 1} &= \mp U_c \left[ \frac{1}{M_{j-1,n}^2} + \frac{1}{L_{j,n\pm 1}^c} \right], \\
 X_{j,n}^{-j,-n} &= -A_a^{*2} \left[ \frac{1}{P_{j+1,n}^a} + \frac{1}{P_{j-1,n}^a} \right], \\
 X_{j,n}^{-j\pm 2,-n} &= A_a^{*2} / P_{j\mp 1,n}^a, \\
 X_{j,n}^{-j-1,-n\pm 1} &= \pm A_a^* A_b^* / M_{j+1,n}^2, \\
 X_{j,n}^{-j+1,-n\pm 1} &= \mp A_a^* A_b^* / M_{j-1,n}^2.
 \end{aligned}$$

The corresponding equations for the  $G_{j,n}$  are

$$\begin{aligned}
 & Y_{jn}^{jn} G_{jn} + Y_{jn}^{j,n+2} G_{j,n+2} + Y_{jn}^{j,n-2} G_{j,n-2} + Y_{jn}^{j+2,n} G_{j+2,n} \\
 & + Y_{jn}^{-2,n} G_{j-2,n} + Y_{jn}^{-1,n-1} F_{j-1,n-1} + Y_{jn}^{j-1,n+1} F_{j-1,n+1} \\
 & + Y_{jn}^{j+1,n-1} F_{j+1,n-1} + Y_{jn}^{j+1,n+1} F_{j+1,n+1} + X_{jn}^{-j,-n} G_{-j,-n}^* \\
 & + X_{jn}^{-j,-n+2} G_{-j,-n+2}^* + X_{jn}^{-j,-n-2} G_{-j,-n-2}^* + X_{jn}^{-j+1,-n+1} F_{-j+1,-n+1}^* \\
 & + X_{jn}^{-j-1,-n+1} F_{-j-1,-n+1}^* + X_{jn}^{-j+1,-n-1} F_{-j+1,-n-1}^* \\
 & + X_{jn}^{-j-1,-n-1} F_{-j-1,-n-1}^* + r_b (\delta_{n,1} - \delta_{n,-1}) \delta_{j,0} = 0.
 \end{aligned} \tag{A2}$$

These equations have nonzero terms only for  $j$  even and  $n$  odd. The following definitions apply in this case:

$$\begin{aligned}
 Y_{j,n}^{j,n} &= L_{j,n}^b + U_b \left[ \frac{1}{P_{j,n+1}^b} + \frac{1}{P_{j,n-1}^b} \right] \\
 & + U_a \left[ \frac{1}{L_{j-1,n}^c} + \frac{1}{L_{j+1,n}^c} \right], \\
 Y_{j,n}^{j,n\pm 2} &= -U_b / P_{j,n\pm 1}^b, \\
 Y_{j,n}^{j\pm 2,n} &= -U_a / L_{j\pm 1,n}^c, \\
 Y_{j,n}^{j\pm 1,n+1} &= \pm U_c^* \left[ \frac{1}{M_{j,n+1}^2} + \frac{1}{L_{j\pm 1,n}^c} \right], \\
 Y_{j,n}^{j\pm 1,n-1} &= \mp U_c^* \left[ \frac{1}{M_{j,n-1}^2} + \frac{1}{L_{j\pm 1,n}^c} \right], \\
 X_{j,n}^{-j,-n} &= -A_b^{*2} \left[ \frac{1}{P_{j,n+1}^b} + \frac{1}{P_{j,n-1}^b} \right],
 \end{aligned}$$

$$X_{j,n}^{-j,-n\pm 2} = A_b^{*2} / P_{j,n\mp 1}^b,$$

$$X_{j,n}^{-j\pm 1,-n-1} = \pm A_a^* A_b^* / M_{j,n+1}^2,$$

$$X_{j,n}^{-j\pm 1,-n+1} = \mp A_a^* A_b^* / M_{j,n-1}^2.$$

Despite the complexity of Eqs. (A1) and (A2), considerable simplification may be achieved by noting certain symmetry properties. First, suppose we interchange the decay rates of levels one and three and at the same time interchange the zero-field population inversions of transitions  $a$  and  $b$ . The other parameters characterizing transitions  $a$  and  $b$  are also exchanged. Then  $F_{ij}$  and  $G_{ij}$  are also exchanged for all  $i$  and  $j$ . Specifically, if

$$\gamma_1 \leftrightarrow \gamma_3,$$

$$A_a \leftrightarrow A_b,$$

$$\xi_a \leftrightarrow \xi_b,$$

$$\nu_a \leftrightarrow \nu_b,$$

$$\omega_{21} \leftrightarrow \omega_{32},$$

$$\beta_a \leftrightarrow \beta_b,$$

$$\beta_c \text{ and } \gamma_2 \text{ are unchanged,}$$

then

$$F_{i,j} \leftrightarrow G_{j,i} \quad (\text{A3})$$

for all  $i$  odd,  $j$  even.

The second symmetry property gives the result that the influence on the laser modes of a group of atoms with velocity  $-v$  is the same as the influence of a group of atoms with velocity  $v$ . This must be the case because the geometry we have assumed is symmetric with respect to the interchange of  $+z$  with  $-z$ . The following two equations are sufficient to ensure this property in our formalism<sup>27</sup>:

$$F_{i,j}(v) = -F_{-i,-j}(-v), \quad (\text{A4})$$

$$G_{i,j}(v) = -G_{-i,-j}(-v). \quad (\text{A5})$$

These equations are verified by noting that  $i, j$ , and  $v$  only occur in the coefficients of  $F_{i,j}$  and  $G_{i,j}$  as the products  $iv$  and  $jv$ , and the inhomogeneous terms in the equations change signs when  $i$  and  $j$  change signs. A consequence of Eqs. (A4) and (A5), if one assumes a symmetric atomic velocity distribution, is that the polarization oscillations may be decomposed into standing waves with spatial dependence  $\sin[(ik_a + jk_b)z]$ .

The third symmetry property involves changing the signs of the detunings. It can be shown using Eqs. (A1) and (A2) that

$$F_{-i,-j}(-\Delta_a, -\Delta_b) = -F_{ij}^*(\Delta_a, \Delta_b) \quad (\text{A6})$$

and

$$G_{-i,-j}(-\Delta_a, -\Delta_b) = -G_{ij}^*(\Delta_a, \Delta_b). \quad (\text{A7})$$

The substitution of Eqs. (A6) and (A7) into the expressions for the gain and the index of refraction shows that the gain does not change and the resonant contribution to the index of refraction changes sign [see Eqs. (3.43) and (3.44)] when the signs of both detunings are changed.

Another property of the equations which can be used to simplify our calculations is demonstrated as follows. We multiply Eq. (A1) by  $A_a$  and multiply Eq. (A2) by  $A_b$ . We note that the phases  $\theta_a$  and  $\theta_b$ , and the Fourier coefficients  $F_{ij}$  and  $G_{ij}$  only occur in products of the form  $A_a F_{ij}$ ,  $A_a^* F_{ij}^*$ ,  $A_b G_{ij}$ , and  $A_b^* G_{ij}^*$ . We define

$$F_{ij}^0 = A_a F_{ij} / |A_a|$$

and

$$G_{ij}^0 = A_b G_{ij} / |A_b|.$$

$F_{ij}^0$  and  $G_{ij}^0$  are independent of  $\theta_a$  and  $\theta_b$ . A phase shift  $\theta_a$  (or  $\theta_b$ ) in  $A_a$  (or  $A_b$ ) causes the negative phase shift in  $F_{ij}$  (or  $G_{ij}$ ). It may be shown from this property that the average gain and index of refraction of the laser medium are unaffected by the phases  $\theta_a$  and  $\theta_b$ .<sup>27</sup> Therefore we can assume for our purposes that  $A_a$  and  $A_b$  are real numbers.

The partial difference equations (A1) and (A2) can be written as a single infinite-dimensional matrix equation. We define

$$f_{j,n} = \begin{cases} F_{jn} & \text{for } j \text{ odd and } n \text{ even,} \\ 0 & \text{for } j+n \text{ even,} \\ G_{jn} & \text{for } j \text{ even and } n \text{ odd.} \end{cases}$$

The nonzero  $f_{jn}$  are then reordered as a vector  $V_m$  where  $m = m(j,n)$ . The index  $m$  increases as the order  $|j| + |n|$  of the Fourier terms increases,

$$m(j,n) > m(p,q)$$

$$\text{if } |j| + |n| > |p| + |q|. \quad (\text{A8})$$

The vector  $V$  is made up alternately of the real and imaginary parts of the  $f_{jn}$ . Calculations using complex arithmetic are not convenient because Eqs. (A1) and (A2) include both the  $f_{jn}$  and their complex conjugates. The matrix equation is

$$MV = r, \quad (\text{A9})$$

where the components of  $r$  are the real and ima-

ginary parts of the nonhomogeneous terms of Eqs. (A1) and (A2). Most rows of  $M$  have 32 real nonzero elements and no row has more than this number.

In the computations,  $\underline{V}$  was evaluated numerically after Eq. (A9) was truncated at order  $l$ ; that is, we set  $f_{jn}=0$  for  $|j| + |n| > l$ . The truncated sparse-matrix equation (A9) could then be solved.

The matrix equation (A9) was solved for the first eight elements of  $\underline{V}$ . These are the real and imaginary parts of  $F_{\pm 1,0}$  and  $G_{0,\pm 1}$ . Figure 16 illus-

trates the ordering of the elements of  $\underline{V}$  that was used in the computations. Sequences of numbers

$$F_{\pm 1,0}(l) \text{ and } G_{0,\pm 1}(l), \quad l = n, n+2, n+4, \dots$$

were computed, where  $l$  is the order of the matrix equation defined above. Convergence at order  $p$  was defined by the convergence of these four complex sequences to within a tolerance at that order.

In practice, the matrix equation was successively truncated at order  $n, n+2, n+4, \dots$  until the relative change

$$\kappa = \text{Max} \{ | \text{Re}[F_{\pm 1,0}(p) - F_{\pm 1,0}(p-2)] / \text{Re}F_{\pm 1,0}(p) |, | \text{Re}[G_{0,\pm 1}(p) - G_{0,\pm 1}(p-2)] / \text{Re}G_{0,\pm 1}(p) | \} < \delta, \quad (\text{A10})$$

where  $\delta$  was some predetermined tolerance. We have converged on the change in  $\text{Re}F_{\pm 1,0}$  and  $\text{Re}G_{0,\pm 1}$  because the laser gain, which we are calculating, depends only on these quantities.

**APPENDIX B: ITERATIVE PROCEDURE FOR INVERTING TWO EQUATIONS WITH TWO UNKNOWNNS**

We wish to find  $x_0$  and  $y_0$  such that  $F(x_0, y_0) = F_0$  and  $G(x_0, y_0) = G_0$ . Values  $x_1$  and  $y_1$  are selected to be as close as possible to  $x_0$  and

$y_0$ . Then numerical estimates are made for  $\partial F / \partial x$ ,  $\partial G / \partial y$ ,  $\partial F / \partial y$ ,  $\partial G / \partial x$  at  $x_1$  and  $y_1$ . The next estimates of  $x_0$  and  $y_0$  are obtained using

$$x_2 = x_1 + \{ \partial G / \partial y [F_0 - F(x_1, y_1)] - \partial F / \partial y [G_0 - G(x_1, y_1)] \} / d, \quad (\text{B1})$$

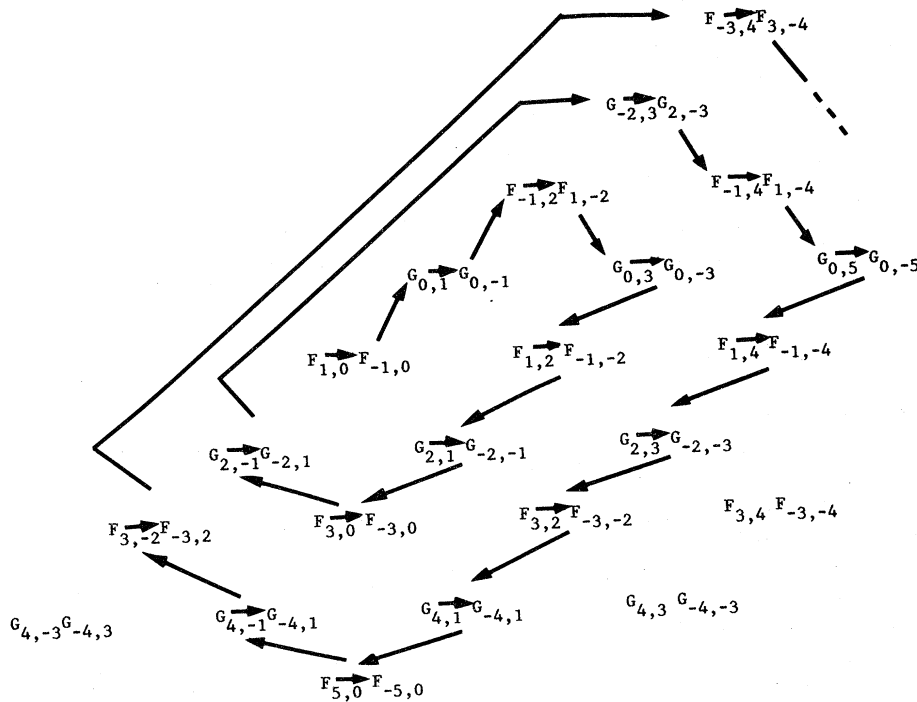


FIG. 16. Ordering of the elements of the vector  $\underline{V}$  Eq. (A9). The first element of the vector is  $F_{1,0}$ .

$$y_2 = y_1 + \{ \partial F / \partial x [G_0 - G(x_1, y_1)] - \partial G / \partial x [F_0 - F(x_1, y_1)] \} / d, \quad (\text{B2})$$

where

$$d = (\partial F / \partial x)(\partial G / \partial y) - (\partial F / \partial y)(\partial G / \partial x). \quad (\text{B3})$$

This procedure is iterated until  $F$  and  $G$  are close

enough to  $F_0$  and  $G_0$ . This algorithm was especially effective in evaluating the graphs shown in Figs. 6 through 14 because the initial estimates for the intensities were obtained from an adjacent point on the graph, except at the first point in each disconnected region of nonzero  $I_a$ . A single iteration was generally adequate to obtain  $x$  and  $y$  such that  $F$  and  $G$  were within 0.3% of  $F_0$  and  $G_0$ , respectively.

\*Current address: Mission Research Corporation, 1720 Randolph Road SE, Albuquerque, New Mexico 87106.

<sup>1</sup>M. Sargent III, M. O. Scully, and W. E. Lamb Jr., *Laser Physics* (Addison-Wesley, Reading, Mass., 1974).

<sup>2</sup>L. Allen and J. H. Eberly, *Optical Resonance and Two-Level Atoms* (Wiley, New York, 1975).

<sup>3</sup>W. E. Lamb, Jr., *Phys. Rev.* **134**, A1429 (1964).

<sup>4</sup>I. M. Beterov and V. P. Chebotayev, in *Progress in Quantum Electronics*, edited by J. H. Sanders and S. Stenholm (Pergamon, Oxford, 1975), Vol. 3, Part 1.

<sup>5</sup>T. Hansch and P. Toschek, *Z. Phys.* **236**, 213 (1970).

<sup>6</sup>R. Salomaa, *J. Phys. B* **10**, 3005 (1977).

<sup>7</sup>V. S. Letokhov and V. P. Chebotayev, *Nonlinear Laser Spectroscopy* (Springer, Berlin, 1977), Chap. 5.

<sup>8</sup>M. S. Feld, in *Frontiers in Laser Spectroscopy*, 1975, Les Houches Lectures, edited by R. Balian, S. Haroche, and S. Liberman (North-Holland, Amsterdam, 1977), Course 3, Vol. 1, p. 206.

<sup>9</sup>F. Najmabadi, M. Sargent III, and F. A. Hopf, *Phys. Rev. A* **12**, 1553 (1975).

<sup>10</sup>H. R. Schlossberg and A. Javan, *Phys. Rev.* **150**, 267 (1966).

<sup>11</sup>M. S. Feld and A. Javan, *Phys. Rev.* **177**, 540 (1969).

<sup>12</sup>T. Ya Popova, A. K. Popov, S. G. Rautian, and R. I. Sokolovskii, *Zh. Eksp. Teor. Fiz.* **57**, 850 (1969) [*Sov. Phys.—JETP* **30**, 466 (1970)].

<sup>13</sup>B. J. Feldman and M. S. Feld, *Phys. Rev. A* **5**, 899 (1972).

<sup>14</sup>E. Kyrölä and R. Salomaa, *Phys. Rev. A* **23**, 1874 (1981).

<sup>15</sup>H. Schlemmer, D. Frolich, and H. Welling, *Opt. Commun.* **32**, 141 (1980).

<sup>16</sup>H. Welling and D. Frölich, in *Festkörperprobleme, Advances in Solid State Physics*, edited by J. Treusch (Vieweg, Braunschweig, 1979), Vol. 19, p. 403.

<sup>17</sup>E. A. Sziklas and A. E. Siegman, *Appl. Opt.* **14**, 1874 (1975).

<sup>18</sup>D. B. Rensch, *Appl. Opt.* **13**, 2546 (1974).

<sup>19</sup>P. W. Milonni and A. H. Paxton, *J. Appl. Phys.* **49**, 1012 (1978).

<sup>20</sup>S. Stenholm and W. E. Lamb, Jr., *Phys. Rev.* **181**, 618 (1969).

<sup>21</sup>W. R. Bennet, Jr., *Appl. Opt. Suppl.* **1**, 24 (1962).

<sup>22</sup>H. R. Schlossberg and A. Javan, *Phys. Rev. Lett.* **17**, 1242 (1966).

<sup>23</sup>A. H. Paxton and P. W. Milonni, *Opt. Commun.* **34**, 111 (1980).

<sup>24</sup>B. J. Feldman and M. S. Feld, *Phys. Rev. A* **1**, 1375 (1970).

<sup>25</sup>S. G. Rautian, *Zh. Eksp. Teor. Fiz.* **51**, 1176 (1966) [*Sov. Phys.—JETP* **24**, 788 (1967)].

<sup>26</sup>P. R. Berman, *Phys. Rev. A* **5**, 927 (1972).

<sup>27</sup>A. H. Paxton, Ph.D. dissertation, University of New Mexico, 1981 (unpublished), available from University Microfilms, Ann Arbor, Michigan, 1981.

<sup>28</sup>A. Javan, in *Proceedings of the International School of Physics "Enrico Fermi", Course XXXI*, Varenna, 1963, edited by P. A. Miles and C. H. Townes (Academic, New York, 1964), p. 284.

<sup>29</sup>A. Javan, *Phys. Rev.* **107**, 1579 (1957)

<sup>30</sup>B. J. Feldman and M. S. Feld, *Phys. Rev. A* **12**, 1013 (1975).

<sup>31</sup>N. Skribanowitz, M. J. Kelly, and M. S. Feld, *Phys. Rev. A* **6**, 2302 (1972).

<sup>32</sup>H. Haken, R. Der Agobian, and M. Pauthier, *Phys. Rev.* **140**, A437 (1965).

<sup>33</sup>The Yale Sparse-Matrix Package developed by A. H. Sherman, S. C. Eisenstat, and M. H. Schultz was used. See A. H. Sherman, *Yale Sparse Matrix Package User's Guide* UCID-30114 (Computer Documentation, Lawrence Livermore Laboratory, University of California, Livermore, Calif., 1975).

<sup>34</sup>G. M. Lawrence and H. S. Liszt, *Phys. Rev.* **178**, 122 (1969).

<sup>35</sup>A. Corney, *Atomic and Laser Spectroscopy* (Oxford University Press, Oxford, 1977), p. 332.